Optimal Routing and Charging of Electric Mobility-on-Demand Systems

A Thesis

Presented in Partial Fulfilment of the Requirements for the

Degree of Master of Science

with a

Major in Electrical Engineering

in the

College of Engineering

University of Idaho

by

Mustafa Ammous

Major Professor: Sameh Sorour, Ph.D.

Committee Members: Ahmed Abdel-Rahim, Ph.D., P.E.; Brian Johnson, Ph.D., P.E.

Department Administrator: Joseph Law, Ph. D., P.E.

August 2018

Authorization to Submit Thesis

This thesis of Mustafa Ammous, submitted for the degree of Master of Science with a major in Electrical and Computer Engineering and titled "Optimal Routing and Charging of Electric Mobility-on-Demand Systems," has been reviewed in final form. Permission, as indicated by the signatures and dates given below, is now granted to submit final copies to the College of Graduate Studies for approval.

Major Professor: _____Date_____
Sameh Sorour, Ph.D.

Committee Members: _____Date_____
Brian Johnson, Ph.D., P.E.

_____Date_____
Ahmed Abdel-Rahim, Ph.D., P.E.

Department Administrator: _____Date_____
Joseph Law, Ph.D., P.E.

Abstract

Mobility-On-Demand (MoD) systems using electric vehicles (EVs) are expected to play a significantly increasing role in the near future of urban transportation systems, to both cope with the massive increases in urban population and reduce carbon emissions. One inconvenience in MoD-EV systems is the need for some customers to charge the vehicles for almost out of charge EVs before reaching their destinations. In this thesis, we propose three different routing models that aim to reduce this inconvenience by minimizing the relative excess time spent by MoD-EV systems customers in charging compared to the on-road trip time. In the first model, the routing problem between multiple MoD-EV stations with in-route charging as a multi-server queuing system is considered. We formulate our objective as a stochastic convex optimization problem that minimizes the average overall trip time for all customers relatively to their actual trip time without in-route charging. Both single and multiple charging units per charging station are considered, and modeled as M/M/1 and M/M/c queues, respectively. In the second model, a cost on the charging is added in the process and the objective is to minimize the total trip time with charging relative to the time without charging as well as reducing the total cost of charging. The problem is modeled also as convex optimization with two objectives, and is solved also for both types of queues M/M/1 and M/M/c. In the third model, two options of charging are considered in the routing scheme of the first model. Customers can charge either at the pick-up locations or perform in-route charging. Obviously, charging all the EVs at the pick-up locations might not be the best solution as the delay may go large or even unbounded. Hence, an optimization problem needs to be solved to determine which customers will charge at the pick-up locations and which will perform in-route charging with the objective to minimize the average total trip time for all the customers. It is modeled also as a convex optimization problem. In all the models, the optimal routing proportions are derived analytically using Lagrangian analysis and Karush-Kuhn-Tucker (KKT) conditions. Simulation results show

the merits of our proposed solution in all cases as compared to the shortest time and the random routing decisions.

Acknowledgements

I would like to thank my thesis advisor Dr. Sameh Sorour for his continuous support in my research and my degree. I would like also to thank my thesis committee Prof. Ahmed and Prof. Brian for their support and review of the thesis content. I am also really thankful for my partner in the research Syrine Belakaria for her helping me in different parts of my research with her amazing analytical skills. Finally, I must express my gratitude to my parents and my friends who continuously supported me during my education journey. This work has been partially funded by the U.S. Department of Transportation's University Transportation Center program, Grant #69A3551747129 through the Center for Safety Equity in Transportation (CSET) Tier-1 University Transportation Center. I would like also to thank the funding agency.

Table of Contents

List of Tables

List of Figures

CHAPTER 1

Introduction

1.1 Motivation

Transportation systems in urban areas are facing many challenges nowadays due to the high demand on private vehicles ownership, which increases road congestion [2], demand on parking spots [3], and harmful emissions to the environment [4]. A recent study from the United Nations expects the urban population to double by 2050 [5]. This fact will definitely increase the demand for private mobility services even more. The metropolitan spatial restrictions will impose strict limitations on constructing new roads and parking spaces that can cope with this increase in private transportation demands. Consequently, the current dependence on personal vehicles for private transportation seems to be an unsustainable and polluting solution for urban mobility in the near future. One promising solution for this problem is the one-way vehicles sharing, widely known as Mobility-On-Demand (MoD) [6]. Using electric vehicles (EVs) for these MoD systems (that we will refer to as MoD-EV) is an even more attractive solution, not only for future private mobility services but also to reduce the emissions of greenhouse gases that cause drastic pollution to the environment [7].

Since EVs are running on electric batteries, they need to be regularly charged. Such charging usually takes relatively and much longer times, using fast and conventional charging units, respectively, than filling up fossil fuel based vehicles with gas. The availability of only slow-charging units and/or less fast-charging units compared to the number of EVs in MoD-EV stations, may frequently result in EVs not having enough time to be sufficiently (or at all) charged before their next pick-up, especially in high demand MoD-EV systems. Indeed, with heavy dependency on such services, many customers may simultaneously encounter instances of needing (if they have no other choices given their tight schedules) or choosing (due to their more relaxed schedules and proper compensation) to use these not-sufficiently charged EVs. Their only alternative to use these EVs is to charge them at

dedicated fast-charging stations so that they can drive them to their destinations. On the other hand, the current limited fast-charging infrastructure in many cities may suffer from large queuing delays if not smartly managed given this high MoD-EV fast-charging demand, especially if they run on renewable energy [8]. These two aspects combined can pose a significant threat to the wide proliferation of MoD-EV systems. Clearly, tight-schedule customers will not be happy with the service if their charging delays make them arrive late to their destinations. Even if the MoD-EV operators allocate such EVs only to delay-tolerant customers in return for compensation (e.g., special discounts on their current or future trips), significant charging delays can still cause high frustration and lack of interest in continuing to use this service.

Consequently, minimizing the average total trip times of these customers and the excess times they spend for the charging of these vehicles, with the respect to the actual on-road trip time, is a crucial point to reduce customer frustration and discouragement in using MoD-EV systems. Such minimization requires real-time knowledge of many system parameters, such as the number/rate of vehicles requesting in-route charging, their origin and destination stations, the possible charging stations, their charging rates, their current queuing times, etc. Luckily, the advancement and near-future deployment of the Internet-of-Things (IoT) and cloud-based smart cities technologies have been enabling the collection of this information at a cloud server, and the optimization of the entire process. Indeed, the cloud server can employ the collected information to direct these vehicles to the different available charging stations so as to balance their loads with respect to their real-time energy supply, and thus reduce the customer excess delays at these stations, relative to their original on-road trip times.

Another influential parameter from the service operator side is the various charging costs of the different charging stations, due to their various charging rates from both local renewable sources and the grid. Consequently, the selections of customers on which charging station they go to, may significantly increase, not only their delays, but also the operator

overall costs for charging. The latter problem can significantly affect the operator's revenues and thus interest in pursuing/proceeding with this business.The only solution to these problems is to exploit the near-future establishment of connected and smart cities. By connecting the operator to the charging stations to collect their real-time energy supply, occupancy, and charging costs, the former can smartly route its customers to the different available charging stations so as to reduce both customer excess delays and cost of charging.

1.2 Related Work

Many works have considered different problems related to EV charging [8, 9, 10], to optimize different metrics such as charging delays and pricing, using different approaches such as queuing networks [9, 10] and Markov decision processes [8]. In [9], a queuing network model was proposed to estimate the charging demand of the EVs at different stations and how the charging prices are affecting the driver decisions on the choice of the stations. In [8, 9], only one EV arrives at a time to each charging station, while in [10] multiple EVs arrive as a platoon to the charging station. The operation of one charging station with multiple charging units was modeled as a multi-server queue in [8] with two different sources of energy; power grid and renewable sources (considered free). The objective was to minimize the overall cost of EV charging in this station. Different works also considered various approaches for EV battery charging, such as charging from the power grid [9], charging from renewable sources [10], a combination of both [8], and battery swapping [11]. Lately, wireless charging was also proposed to further reduce charging delays at the expense of high installation costs for equipment and infrastructure [12]. In [11], a charging station equipped with battery swapping technology was modeled as a network with two queues; an open queue of the EVs and a closed queue of the batteries. This system was tested for different numbers of EV arrivals and batteries to evaluate the performance of battery swapping stations. Moreover, several parameters were measured like the probability of being not served, number of busy chargers,

and waiting time. In [13], a new method was proposed for the optimal load scheduling of plug-in hybrid EVs mainly to optimize two objectives; the peak-to-valley difference and the economic loss and then solved algorithmically. In [14], another method for scheduling and centralized charging for EVs was proposed again to optimize power losses, overload, voltage fluctuation and charging costs on the power grid.

Other works have considered the routing of EVs to minimize the costs, improve battery lifetime [15][16], or safely reach a charging station [17]. In [15], the proposed model aimed to optimize the routing of airport shuttles which operate on electric battery, and each having a fixed schedule. However, none of these prior works focused on the relation between routing and charging.

In [18], a joint routing and charging reservation scheme was analyzed to minimize the overall trip delay. However, the reservation-based charging model was very simplistic and did not capture the real dynamics of queues at charging stations. On the other hand, recent works have considered MoD systems and its autonomous driving version, known as autonomous MoD (AMoD) [6, 19]. However, these works mainly considered the re-balancing problem of vehicles between the different passenger stations [6], and AMoD fleet sizing [19], and no EVs charging issues were considered. In [20], the authors' objective is to re-balance MoD systems while minimizing the cost of re-balancing (car relocation). In [21], scheduling algorithm for MoD-EV systems was discussed. The authors objective was to maximize the number customers using the EVs based on a reservation system one day before any trip while optimizing also the charging of EVs during the day. In [22], a model for optimizing the fleet size of car-sharing system at different pickup locations were discussed. In [23], the joint dispatching and charging of AMoD EVs was studied, but without any routing nor in-route charging issues. In both [6, 23], the systems were modeled as queuing networks with different objectives (minimizing the number of re-balancing vehicles in the roads [6] and minimizing the response time of EV assignment to customers [23]) and both problems were solved using linear programming techniques. In [24], different machine intelligence algorithms were

discussed for implementation and testing on fully automated cars which is the future of transportation and MoD.

Finally, recent works have employed the connectivity capabilities of transportation and smart grid infrastructure to safely navigate vehicles to charging station and provision enough energy resources to charge them [17]. The moving EVs that require charging send a request to road-side-units (RSUs), which route them to charging stations (not necessarily their nearest ones) based on the current available data from the RSUs and the load on the charging stations to avoid overloading the power grid [17]. However, this work did not consider any optimization of charging delays, nor excess charging times.

1.3 Our Contribution

In this thesis, we focus on the routing of MoD EVs between a group of passenger stations, while each of them needs charging in one of multiple available charging stations with different energy resources. Customers with less delay constraints are allocated to these EVs but still require to have the minimal increase in their trip times to charge these EVs. Similar to [17], the system will harness the emergent ubiquitous connectivity and cloud technology to enable the real-time collection of EV state-of-charge information, departure rates from passenger stations, energy supplies at different stations, and trip times without charging. The cloud server will then make decisions on the proportions of EVs routed from each of the passenger stations to each charging station, so as to minimize the expected overall trip time for all customers over all routes relative to their trip time without charging. We propose three different models in this thesis.

In the first model, customer can perform in-route charging in the multiple charging stations available in the city. However, they need to have the minimal increase in their trip time to reach the destination. Two charging station settings are considered, namely the single and multiple charging unit stations, which both exist in practical life. To solve

this problem, we first model the system as a multi-server queuing network, where each server represents one of the possible charging stations. We further model the two considered settings for each charging station by M/M/1 and M/M/c queuing systems, respectively. We then employ this model to formulate the aforementioned problem as a convex optimization over stochastic decision variables, representing EV routing proportions between each pair of passenger stations through the different charging stations. Expressions of the optimal routing proportions are derived using Lagrangian analysis and Karush-Kuhn-Tucker (KKT) conditions. The derived optimized routing proportions are tested for a wide variation range of the different system parameters and different charging approaches (i.e., direct charging and battery swapping) through extensive simulations. The overall expected trip times and excess delay percentages due to charging using our optimized routing proportions are compared to conventional shortest time and random routing decisions for both M/M/1 and M/M/c charging station models. Finally, the proposed routing method is tested on a real-world scenario and the computation times for the different settings are discussed.

In the second model, a cost on the charging is added to the first model. Hence, there are two objectives now to minimize the overall expected trip times for all the customers relative to their trip times without charging as well as minimizing the charging costs from the operator side. Two settings of charging station are also considered M/M/1 and M/M/c. The problem is formulated as dual objective convex optimization problem with convex constraints. Similar to the first model, the Lagrangian analysis and KKT conditions are used to provide analytical solutions for the routing proportions. The performance of this model is tested through extensive simulations for different parameters to evaluate the model. The model is also compared to other routing schemes and is tested on a real-world scenario.

In the third model, two options of charging are considered in the first model. Customers can charge at the pick-up location or perform in-route charging. Clearly, charging all the EVs at the pick-up location might not be the best solution as the delay may go large. The traffic conditions on different roads are considered in this model. The problem is formulated as a

convex optimization problem with objective to minimize the average trip times for all the customers relative to their trip times without charging. Again, the problem is solved using Lagrangian analysis and KKT conditions to find the analytical solutions for the optimization variables. It is tested then using simulations to evaluate the performance of the model with different system parameters and comparing it to other routing schemes.

CHAPTER 2

Optimal Routing with In-Route Charging Of MoD-EV Systems

This chapter discusses the issue of the in-route charging only where the customers need to charge EVs before reaching their destination. The problem is formulated using queuing theory based on M/M/1 and M/M/c queues and then solved analytically and numerically to illustrate the performance of the proposed method.

2.1 System Model

This thesis considers the MoD-EV system in Figure 2.1, with n passenger stations (PSs) and m charging stations (CSs). PSs are the locations at which customers pick-up EVs close to their origin and drop them off close to their destinations. The model only considers EVs that need to be charged on the way to the destination by less time-constrained customers. These customers and EVs are modeled by arrival and service queues, respectively, in each PS as illustrated in Figure 2.1. Each charging station is also modeled by a queuing system, as also illustrated in Figure 2.1. This queuing system can be either an M/M/1 or M/M/c queuing model for all the charging stations in the system. Clearly, the M/M/1 model is a special case of the general M/M/c, and both of them will be considered separately in the analysis.

Similar to [6, 9], the overall departure rate of these EVs from PS i is modeled by a Poisson process with rate λ_i EVs / unit time. When departing, each customer intends to go to PS j with probability q_{ij} ($q_{ii} = 0$). On the other hand, each (or the only) charging unit in CS k can complete either the direct EV charging or the swapping of its battery [11, 18] in an exponentially distributed duration with rate μ_k EVs / unit time per server similar to [11, 25], which is different from one CS to another given their different supplies of energy. Finally, the real-time trip duration between PSs i and j through CS k, without charging, is denoted by $t_{ij}^{(k)}$. Table 2.1 summarizes the different parameters considered in our model.

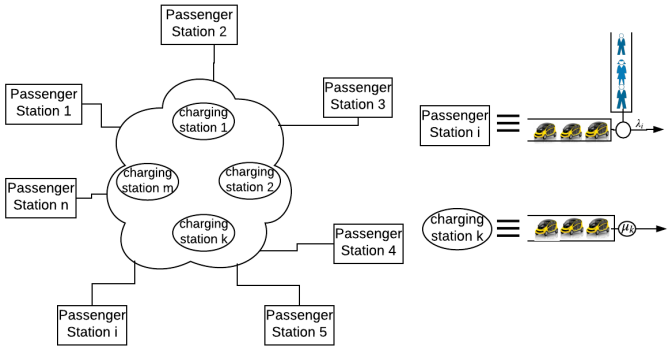

Figure 2.1: General model of a city with n passenger stations and m charging stations showing the queues at each passenger station and charging station.

Table 2.1: List of System and Decision Parameters

Parameter	**Definition**
n:	Total number of PSs
m:	Total number of CSs
λ_i:	Departure rate from PS i
q_{ij}:	Probability for customer to go from PS i to PS j
μ_k:	Charging or battery-swapping rate at CS k per server
$t_{ij}^{(k)}$:	Time spent on the road only from PS i to PS j through CS k without considering the charging time
$P_{ij}^{(k)}$:	Routing proportion from PS i to PS j through CS k
c:	Total number of servers at each CS k
$\tau_{ij}^{(k)}$:	Actual trip time from PS i to PS j through CS k including charging
$T_{ij}^{(k)}$:	An upper bound on $\tau_{ij}^{(k)}$

The charging rates μ_k at each charging station regularly changes depending on the status of the storage devices and the arrivals of energy to each of them. In addition, $t_{ij}^{(k)}$ also changes due to natural changes of traffic conditions at different times of the day. Given the trendy ubiquitous connectivity through IoT, a cloud controller similar to the one in Figure 2.2 can periodically collect all the above parameters in real-time given time-varying charging and traffic conditions (and thus time-varying of μ_k and $t_{ij}^{(k)}$ $\forall$ i, j, k), and predicts the requests at the PSs based on previous data. The cloud controller will then employ this collected information in guiding EVs departing from PS i towards PS j to route through and charge

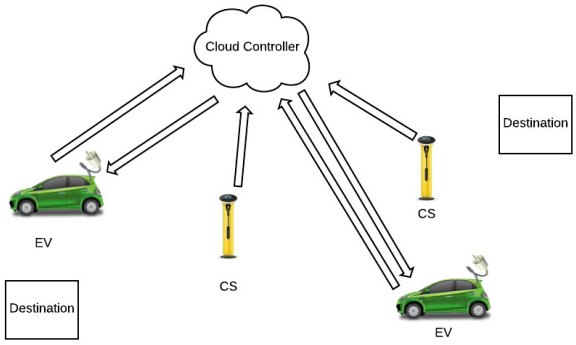

Figure 2.2: Cloud controller to assign routing proportions to the EVs.

at CS k with a routing proportion $P_{ij}^{(k)}$. It is easy to see that:

$$\sum_{k=1}^{m} P_{ij}^{(k)} = q_{ij} \ \forall \ i, j \text{ and } i \neq j \tag{2.1}$$

$$\sum_{\substack{j=1 \\ i \neq j}}^{n} \sum_{k=1}^{m} P_{ij}^{(k)} = 1 \ \forall \ i \tag{2.2}$$

Equation (2.1) shows that the sum of the proportions $P_{ij}^{(k)}$ for specific origin PS i and destination PS j over all the charging stations equals to q_{ij} (i.e. the portions of EVs traveling between i and j through all possible CSs should be equal to portion of customers requesting this route). Equation (2.2) shows that the sum of all proportions $P_{ij}^{(k)}$ leaving each PS equals 1 (i.e., the number of EVs leaving PS i must equal to portion of customers requesting to travel from PS i, which is 100%).

The routed EVs from all PSs to CS k queue up to charge, thus acquiring excess delays in these CSs on top of the actual trip time $t_{ij}^{(k)}$ without charging. After departing from the CS, EVs continue their routes to their destination PSs. The cloud server is thus required to periodically determine these proportions $P_{ij}^{(k)}$, given the real-time values of λ_i, q_{ij}, μ_k, and $t_{ij}^{(k)} \ \forall \ i, j, k$, in order to minimize the average total trip time of all customers through any route relative to its $t_{ij}^{(k)}$ value $\forall \ i, j, k$.

Clearly, the conventional shortest time routing strategy, which routes a customer departing from PS i and destined to PS j through CS $k = \arg\min_k \left\{ t_{ij}^{(k)} \right\}$ may not necessarily be the best strategy since the CS in this route might be overloaded or having insufficient charging rate, and will thus result in an extremely large (or even unbounded) charging delay. The question that the cloud server should periodically resolve is: *Which stochastic routing strategy should be followed in each period (given the collected real-time values of the different system parameters) in order to minimize the overall average trip time between any pair of PSs, as well as the excess percentage of times wasted by customers in CSs, relative to the actual trip times without charging.*

Given this system model described above, and well-known thinning properties of Poisson processes, the arrival process to the queue of each CS k is an independent Poisson process with rate λ_k, which can be expressed as:

$$\lambda_k = \sum_{\substack{i=1 \\ i \neq j}}^{n} \sum_{j=1}^{n} \lambda_i P_{ij}^{(k)} \tag{2.3}$$

This expression is obtained for CS k by summing the rates of all thinned departure processes from each PS i whose rate is $\lambda_i P_{ij}^{(k)}$.

It is important to note that this paper assumes customers' compliance with the optimized routing proportions suggested to them by the system. However, the extension of the solution to cases of customer incompliance, which are indeed possible to occur in reality, can be done by our suggested cloud and IoT enabled system. Indeed, such incompliances can be easily detected through the collected GPS information from the EVs or their charging at other CSs than the ones they were directed to go to. The system can thus resolve these situations by either making corrective adjustments to subsequent EV routing so as to maintain the optimized proportions, or re-running the optimization algorithm if drastic changes to the system parameters were detected. The system can also reduce these incompliance events by informing customers who chose to use such EVs for discounted prices that their discounts

will be reduced if they do not comply.

2.2 M/M/1 CS Model

In this section, we will first formulate our problem of interest while assuming that all CSs consists of a single charging unit, and thus can be modeled as M/M/1 queues. The optimal routing proportions for this problem will then be derived using Lagrangian analysis and KKT conditions.

2.2.1 Stability Constraints

Since the arrival process to each CS k is Poisson with rate λ_k and the charging duration at each CS k are exponentially distributed with rate μ_k, the overall queuing system at each CS k becomes an M/M/1 queue [26]. Consequently, the entire system becomes a multi-server queuing system consisting of m independent CS M/M/1 queues, with different arrival rates depending on the routing proportions $P_{ij}^{(k)}$, $\forall\ i, j, k$, and different service rates due to their energy supplies. To ensure the stability of each CS k queue, the arrival rate to this CS k must be strictly less than its service rate μ_k. That is:

$$\sum_{\substack{i=1 \\ i \neq j}}^{n} \sum_{j=1}^{n} \lambda_i P_{ij}^{(k)} < \mu_k \ \forall\ k \tag{2.4}$$

By summing the left-hand sides and right-hand sides of the inequalities (2.4) for all k, we get the general stability condition of the entire queuing system, expressed as:

$$\sum_{i=1}^{n} \lambda_i \ < \ \sum_{k=1}^{m} \mu_k \tag{2.5}$$

In other words, the sum of the departure rates from all PSs must be strictly less than the sum of all charging rates at all CSs to ensure the stability of the entire queuing system.

Now from a practical operation point of view, What if the requests of charging are more than what the CSs can handle? The considered cloud-based management system in this paper can handle such scenarios of higher demand on EV requiring in-route charging compared to the overall charging rates. Since the system is connected to both the customer service apps, EVs, and the charging stations, it can determine the maximum number of EVs that can charge in-route using the derived stability conditions, and block any further request of such EVs if the demand surpasses this maximum number.

2.2.2 Problem Formulation

From basic analysis of M/M/1 queues [26], the expected charging time (denoted by D_k) at each CS k can be expressed as :

$$D_k = \frac{1}{\mu_k - \sum_{i=1}^{n} \sum_{\substack{j=1 \\ i \neq j}}^{n} \lambda_i P_{ij}^{(k)}} \ \forall \ k \tag{2.6}$$

Therefore, the total expected trip time $\left(\text{denoted by } \tau_{ij}^{(k)}\right)$ from PS i to PS j through CS k with in-route charging can be expressed as:

$$\tau_{ij}^{(k)} = t_{ij}^{(k)} + \frac{1}{\mu_k - \sum_{i=1}^{n} \sum_{\substack{j=1 \\ i \neq j}}^{n} \lambda_i P_{ij}^{(k)}} \ \forall \ i, j, k \tag{2.7}$$

As stated earlier, the main objective of our routing proportion optimization is to minimize the expected overall trip time for all customers over all routes, relative to their trip time without in-route charging, while respecting the stability constraints of the system. We can now introduce a new variable $T_{ij}^{(k)}$ which is an upper bound on the actual trip time $\tau_{ij}^{(k)}$ (i.e. $\tau_{ij}^{(k)} \leq T_{ij}^{(k)}$). By minimizing the upper bound $T_{ij}^{(k)}$, we ensure that the actual trip time $\tau_{ij}^{(k)}$

is also minimized. This problem can be formulated as follows:

$$\underset{P_{ij}^{(k)} \forall i,j,k}{\text{minimize}} \quad \sum_{\substack{i=1 \\ i \neq j}}^{n} \sum_{j=1}^{n} \sum_{k=1}^{m} \frac{T_{ij}^{(k)}}{t_{ij}^{(k)}} \tag{2.8a}$$

$$s.t. \quad t_{ij}^{(k)} + \frac{1}{\mu_k - \sum_{\substack{i=1 \\ i \neq j}}^{n} \sum_{j=1}^{n} \lambda_i P_{ij}^{(k)}} \leq T_{ij}^{(k)} \ \forall \ i, j, k \tag{2.8b}$$

$$\sum_{k=1}^{m} P_{ij}^{(k)} = q_{ij} \ \forall \ i, j \tag{2.8c}$$

$$\sum_{\substack{j=1 \\ i \neq j}}^{n} \sum_{k=1}^{m} P_{ij}^{(k)} = 1 \ \forall \ i \tag{2.8d}$$

$$0 \leq P_{ij}^{(k)} \ \forall \ i, j, k \tag{2.8e}$$

$$T_{ij}^{(k)} > t_{ij}^{(k)} \ \forall \ i, j, k \tag{2.8f}$$

Constraints (2.8b) combined with the objective function guarantee the achievement of the desired goal $\left(\text{minimizing } \tau_{ij}^{(k)} \text{ relative to } t_{ij}^{(k)}\right)$ in a weighted epigraph form [27]. Constraints (2.8c) and (2.8d) represent the facts in equations (2.1) and (2.2), respectively, on the routing proportions $P_{ij}^{(k)}$. Constraint (2.8e) guarantees that each routing proportion is always greater than or equal to 0 and constraint (2.8c) guarantees that each routing proportion is always equal or less than $q_{ij}^{(k)}$, while Constraint (2.8f) guarantees the positivity of the charging delay D_k.

By re-arranging (2.8b), we get:

$$\sum_{\substack{i=1 \\ i \neq j}}^{n} \sum_{j=1}^{n} \lambda_i P_{ij}^{(k)} \leq \mu_k - \frac{1}{T_{ij}^{(k)} - t_{ij}^{(k)}} \ \forall \ i, j, k \tag{2.9}$$

Consequently, the problem in (2.8) becomes a convex optimization problem with linear objective function and convex constraints. Moreover, (2.8f) guarantees the strict positivity of the second term of the right-hand side of (2.9), thus making the latter ensure the stability

of the system.

2.2.3 Optimal Routing Proportions

Since the problem in (2.8) is convex, it satisfies Slater's theorem. Thus, strong duality holds and the solutions of the primal and dual problems are identical [27]. Furthermore, the KKT conditions provide necessary and sufficient conditions for optimality [27]. The Lagrangian function corresponding to (2.8) is given in equation (2.10), where $\alpha_{ij}^{(k)}$, $\beta_{ij}^{(k)}$, γ_{ij}, ω_i and $\chi_{ij}^{(k)}$ are the Lagrange multipliers associated with the different problem constraints.

$$
\begin{aligned}
L(P,T,\alpha,\beta,\gamma,\omega,\zeta,\chi) &= \sum_{\substack{i=1\\ i\neq j}}^{n}\sum_{j=1}^{n}\sum_{k=1}^{m}\frac{T_{ij}^{(k)}}{t_{ij}^{(k)}} \\
&+ \sum_{\substack{i=1\\ i\neq j}}^{n}\sum_{j=1}^{n}\sum_{k=1}^{m}\left(\alpha_{ij}^{(k)}\left(\sum_{\substack{i=1\\ i\neq j}}^{n}\sum_{j=1}^{n}\lambda_i P_{ij}^{(k)} + \frac{1}{T_{ij}^{(k)}-t_{ij}^{(k)}} - \mu_k\right)\right) \\
&+ \sum_{\substack{i=1\\ i\neq j}}^{n}\omega_i\left(\left(\sum_{j=1}^{n}\sum_{k=1}^{m}P_{ij}^{(k)}\right)-1\right) + \sum_{\substack{i=1\\ i\neq j}}^{n}\sum_{j=1}^{n}\sum_{k=1}^{m}\left(-\chi_{ij}^{(k)}P_{ij}^{(k)}\right) \\
&+ \sum_{\substack{i=1\\ i\neq j}}^{n}\sum_{j=1}^{n}\sum_{k=1}^{m}-\beta_{ij}^{(k)}\left(T_{ij}^{(k)}-t_{ij}^{(k)}\right) \\
&+ \sum_{\substack{i=1\\ i\neq j}}^{n}\sum_{j=1}^{n}\gamma_{ij}\left(\left(\sum_{k=1}^{m}P_{ij}^{(k)}\right)-q_{ij}\right)
\end{aligned}
\tag{2.10}
$$

In addition, the following expressions are derived by applying the KKT conditions on the inequality and equality constraints (2.8b)-(2.8f).

$$\alpha_{ij}^{(k)^*}\left(\sum_{\substack{i=1\\ i\neq j}}^{n}\sum_{j=1}^{n}\lambda_i P_{ij}^{(k)^*}+\frac{1}{T_{ij}^{(k)^*}-t_{ij}^{(k)}}-\mu_k\right)=0\ \forall\ i,j,k \tag{2.11a}$$

$$-\beta_{ij}^{(k)^*}(T_{ij}^{(k)^*}-t_{ij}^{(k)})=0\ \forall\ i,j,k \tag{2.11b}$$

$$\chi_{ij}^{(k)^*}P_{ij}^{(k)^*}=0\ \forall\ i,j,k \tag{2.11c}$$

$$\sum_{j=1}^{n}\sum_{k=1}^{m}P_{ij}^{(k)^*}-1=0\ \forall\ i \tag{2.11d}$$

$$\sum_{k=1}^{m}P_{ij}^{(k)^*}-q_{ij}=0\ \forall\ i,j \tag{2.11e}$$

$$\alpha_{ij}^{(k)^*}\geq 0,\ \beta_{ij}^{(k)^*}\geq 0,\ \chi_{ij}^{(k)^*}\geq 0 \tag{2.11f}$$

From equation (2.10), and the fact that the gradient of the Lagrangian function equals 0 at the optimal solution, we obtain the following equations:

$$\frac{1}{t_{ij}^{(k)}}-\frac{\alpha_{ij}^{(k)^*}}{(T_{ij}^{(k)^*}-t_{ij}^{(k)})^2}-\beta_{ij}^{(k)^*}=0\ \forall\ i,j,k \tag{2.12a}$$

$$\lambda_i\left(\sum_{\substack{i=1\\ i\neq j}}^{n}\sum_{j=1}^{n}\alpha_{ij}^{(k)^*}\right)+\gamma_{ij}^{*}+\omega_i^{*}-\chi_{ij}^{(k)^*}=0\ \forall\ i,j,k \tag{2.12b}$$

It is clear from (2.11b) that $\beta_{ij}^{(k)^*}=0$ since $\left(T_{ij}^{(k)^*}-t_{ij}^{(k)}\right)>0$. From equation (2.12a), we get the optimal value of $T_{ij}^{(k)^*}$:

$$T_{ij}^{(k)^*}=\sqrt{\alpha_{ij}^{(k)^*}t_{ij}^{(k)}}+t_{ij}^{(k)}\ \forall i,j,k \tag{2.13}$$

Multiplying equation (2.12b) by $P_{ij}^{(k)^*}$ we get :

$$P_{ij}^{(k)^*}\left(\lambda_i(\sum_{\substack{i=1\\ i\neq j}}^{n}\sum_{j=1}^{n}\alpha_{ij}^{(k)^*})+\gamma_{ij}^*+\omega_i^*-\chi_{ij}^{(k)^*}\right)=0 \tag{2.14}$$

From equation (2.11c), we can find that $\chi_{ij}^{(k)^*}P_{ij}^{(k)^*}=0$. $P_{ij}^{(k)^*}$ that is multiplied by γ_{ij}^* and ω_i^* is replaced by $\left(q_{ij}-\sum_{\substack{u=1\\ u\neq k}}^{m}P_{ij}^{(u)^*}\right)$. Substituting these in (2.14) and by rearrangement, we get the optimal routing proportions as:

$$P_{ij}^{(k)^*}=\max\left(0\ ,\ \frac{-\left(q_{ij}-\sum_{\substack{u=1\\ u\neq k}}^{m}P_{ij}^{(u)^*}\right)\left(\gamma_{ij}^*+\omega_i^*\right)}{\sum_{i=1}^{n}\sum_{j=1}^{n}\alpha_{ij}^{(k)^*}}\right) \tag{2.15}$$

$$\forall\ i,j,k$$

Note that the second term in equation (2.15) was always found to be positive in all tested scenarios (by all tested scenarios, we mean the simulation results), due to the fact that $(\gamma_{ij}^*+\omega_i^*)$ is negative and thus makes the term positive. However, we use the form in (2.15) to set the routing proportion to zero in the rare case of having the second term negative (in all of our simulations, we have not got a zero routing proportion but the expression is written in this way in order to avoid having negative proportions). Finally, (2.13) and (2.15) are the optimal solutions for the Lagrangian function. From Slater's theorem, strong duality holds, and thus (2.13) and (2.15) are the optimal solutions of the original problem in (2.8) [27].

2.3 M/M/c CS Model

In this section, we extend the steps of Section 2.2 to solve our problem of interest given that each CS has c charging units. In this case, each CS can be modeled as an M/M/c queue.

2.3.1 Stability Constraints

Similar to the M/M/1 model explained in Section 2.2, the arrival process to each CS k is Poisson with rate λ_k as shown in equation (2.3). Here, each CS consists of c servers and each server has an exponentially charging rate μ_k at CS k. The charging rate μ_k for each server is the same in each CS and may differ from one CS to another depending on the available energy sources at each CS. Consequently, the entire system becomes a multi-server queuing system consisting of m independent CS M/M/c queues, with different arrival rates depending on the routing proportions $P_{ij}^{(k)}$, $\forall\ i, j, k$, and different service rates. To ensure the stability of each CS k queue, the arrival rate to this CS k must be strictly less than its total service rate $c\mu_k$. That is:

$$\sum_{\substack{i=1 \\ i \neq j}}^{n} \sum_{j=1}^{n} \lambda_i P_{ij}^{(k)} < c\mu_k \ \forall\ k \tag{2.16}$$

The general stability condition of the whole queuing system can be found in a similar way to the M/M/1 model from equation (2.16) and is represented by:

$$\sum_{i=1}^{n} \lambda_i \ < \ \sum_{k=1}^{m} c\mu_k \tag{2.17}$$

Similar to the M/M/1 model, if the demand on charging is too high (CSs can not charge all the EVs requesting in-route charging), then the system will block the extra requests.

2.3.2 Problem Formulation

From basic analysis of M/M/c queues [28], the expected charging time (denoted by D_{c-k}) at each CS k can be expressed by:

$$D_{c-k} = \frac{\dfrac{1}{(c\mu_k - \lambda_k)}}{\left(1 + \left(\dfrac{c!\,(c\mu_k - \lambda_k)}{c\mu_k\,(\lambda_k/\mu_k)^c}\right)\left(\sum_{h=0}^{c-1}\dfrac{(\lambda_k/\mu_k)^h}{h!}\right)\right)} + \frac{1}{\mu_k}\ \forall\ k \tag{2.18}$$

Therefore, the total expected trip time $\left(\text{denoted by } \tau_{ij}^{(k)}\right)$ from PS i to PS j through CS k with in-route charging can be expressed as:

$$\tau_{ij}^{(k)} = t_{ij}^{(k)} + D_{c-k}\ \forall\ i, j, k \tag{2.19}$$

Given the above expressions and the stability constraints of the system, the problem can be formulated for the M/M/c CS model as follows:

$$\underset{P_{ij}^{(k)}\forall i,j,k}{\text{minimize}} \quad \sum_{\substack{i=1\\ i\neq j}}^{n}\sum_{j=1}^{n}\sum_{k=1}^{m}\frac{T_{ij}^{(k)}}{t_{ij}^{(k)}} \tag{2.20a}$$

$$s.t. \quad t_{ij}^{(k)} + D_{c-k} \leq T_{ij}^{(k)}\ \forall\ i, j, k \tag{2.20b}$$

$$\sum_{\substack{i=1\\ i\neq j}}^{n}\sum_{j=1}^{n}\lambda_i P_{ij}^{(k)} < c\mu_k\ \forall\ k \tag{2.20c}$$

$$\sum_{k=1}^{m} P_{ij}^{(k)} = q_{ij}\ \forall\ i, j \tag{2.20d}$$

$$\sum_{\substack{j=1\\ i\neq j}}^{n}\sum_{k=1}^{m} P_{ij}^{(k)} = 1\ \forall\ i \tag{2.20e}$$

$$0 \leq P_{ij}^{(k)}\ \forall\ i, j, k \tag{2.20f}$$

$$T_{ij}^{(k)} > t_{ij}^{(k)}\ \forall\ i, j, k \tag{2.20g}$$

Constraints (2.20b) combined with the objective function guarantee the achievement of

our goal in a weighted epigraph form. Since the reciprocal of the delay function D_{c-k} is a concave function [29] for constant u_k and c, and since the reciprocal of a positive concave function is convex [30], then Constraint (2.20b) is convex. Constraints (2.20d)-(2.20g) are the same as constraints (2.8c)-(2.8f) in the M/M/1 formulation, and are all linear. Constraints (2.20c) and (2.20g) guarantee the stability of the queuing system and are also all linear. Consequently, the problem in (2.20) is a convex optimization problem with linear objective function and convex constraints.

2.3.3 Optimal Routing Proportions

Similar to Section 2.2.3, the problem (2.20) satisfies Slater's conditions as it is a convex problem. Hence, strong duality holds, the solutions of the primal and and dual problems are identical, and the KKT conditions provide necessary and sufficient conditions for optimality [27]. The Lagrangian function for the problem in (2.20) is given by Equation (2.21), where $\nu_{ij}^{(k)}$, η_k, $\xi_{ij}^{(k)}$, κ_{ij}, σ_i and $\psi_{ij}^{(k)}$ are the Lagrange multiplies for the different constraints in (2.20).

$$
\begin{aligned}
L(P,T,\nu,\eta,\xi,\kappa,\rho,\psi,\sigma) = &\sum_{\substack{i=1\\ i\neq j}}^{n}\sum_{j=1}^{n}\sum_{k=1}^{m}\frac{T_{ij}^{(k)}}{t_{ij}^{(k)}} + \sum_{\substack{i=1\\ i\neq j}}^{n}\sum_{j=1}^{n}\sum_{k=1}^{m}\left(\nu_{ij}^{(k)}\left(\sum_{\substack{i=1\\ i\neq j}}^{n}\sum_{j=1}^{n}t_{ij}^{(k)} + D_{c-k} - T_{ij}^{(k)}\right)\right)\\
&+\sum_{k=1}^{m}\left(\eta_k\sum_{\substack{i=1\\ i\neq j}}^{n}\sum_{j=1}^{n}\lambda_i P_{ij}^{(k)} - c\mu_k\right) + \sum_{\substack{i=1\\ i\neq j}}^{n}\sum_{j=1}^{n}\sum_{k=1}^{m}\left(-\psi_{ij}^{(k)}P_{ij}^{(k)}\right) + \sum_{\substack{i=1\\ i\neq j}}^{n}\sum_{j=1}^{n}\sum_{k=1}^{m}-\xi_{ij}^{(k)}\left(T_{ij}^{(k)} - t_{ij}^{(k)}\right)\\
&+\sum_{\substack{i=1\\ i\neq j}}^{n}\sum_{j=1}^{n}\kappa_{ij}\left(\left(\sum_{k=1}^{m}P_{ij}^{(k)}\right) - q_{ij}\right) + \sum_{\substack{i=1\\ i\neq j}}^{n}\sum_{j=1}^{n}\sum_{k=1}^{m}\left(-\psi_{ij}^{(k)}P_{ij}^{(k)}\right) + \sum_{\substack{i=1\\ i\neq j}}^{n}\sigma_i\left(\left(\sum_{j=1}^{n}\sum_{k=1}^{m}P_{ij}^{(k)}\right) - 1\right)
\end{aligned}
\tag{2.21}
$$

In addition, the following expressions are obtained by applying the KKT conditions on the optimization problem in (2.20).

$$\nu_{ij}^{(k)^*}\left(t_{ij}^{(k)} + D_{c-k} - T_{ij}^{(k)^*}\right) = 0 \;\forall\; i,j,k \tag{2.22a}$$

$$\eta_k^*\left(\sum_{\substack{i=1\\ i\neq j}}^{n}\sum_{j=1}^{n}\lambda_i P_{ij}^{(k)^*} - c\mu_k\right) = 0 \;\forall\; k \tag{2.22b}$$

$$-\xi_{ij}^{(k)^*}\left(T_{ij}^{(k)^*} - t_{ij}^{(k)}\right) = 0 \;\forall\; i,j,k \tag{2.22c}$$

$$\psi_{ij}^{(k)^*} P_{ij}^{(k)^*} = 0 \;\forall\; i,j,k \tag{2.22d}$$

$$\sum_{j=1}^{n}\sum_{k=1}^{m} P_{ij}^{(k)^*} - 1 = 0 \;\forall\; i \tag{2.22e}$$

$$\sum_{k=1}^{m} P_{ij}^{(k)^*} - q_{ij} = 0 \;\forall\; i,j \tag{2.22f}$$

$$\nu_{ij}^{(k)^*} \geq 0,\; \eta_k^* \geq 0,\; \xi_{ij}^{(k)^*} \geq 0,\; \psi_{ij}^{(k)^*} \geq 0 \tag{2.22g}$$

From equation (2.21) and the fact that the gradient of the Lagrangian function equals 0 at the optimal solution, we obtain equations (2.23) and (2.24).

$$\frac{1}{t_{ij}^{(k)}} - \nu_{ij}^{(k)^*} - \xi_{ij}^{(k)^*} = 0 \;\forall\; i,j,k \tag{2.23}$$

$$\kappa_{ij}^* - \psi_{ij}^{(k)^*} + \sigma_i^* + \left(\sum_{\substack{i=1\\ i\neq j}}^{n}\sum_{j=1}^{n}\nu_{ij}^{(k)^*}\right)\times$$

$$\left(\frac{\lambda_i q - (c\mu_k - \lambda_k)\left(\frac{-\lambda_i}{c\mu_k}\left(\frac{c!}{a^c}\right)\sum_{h=0}^{c-1}\left(\frac{a^h}{h!}\right) - \frac{c\lambda_i}{\mu_k}\frac{c!}{a^{c+1}}\left(1-\frac{a}{c}\right)\sum_{h=0}^{c-1}\left(\frac{a^h}{h!}\right) + \frac{\lambda_i}{\mu_k}\left(1-\frac{a}{c}\right)\left(\frac{c!}{a^c}\right)\sum_{h=1}^{c-1}\left(\frac{a^h}{h!}\right)\right)}{q^2}\right) = 0$$

$$where\ \lambda_k = \sum_{\substack{i=1\\ i\neq j}}^{n}\sum_{j=1}^{n}\lambda_i P_{ij}^{(k)^*}\ \ a = \frac{\lambda_k}{\mu_k}\ and\ q = \left(c\mu_k - \lambda_k\right)\left(1 + \left(1-\frac{a}{c}\right)\left(\frac{c!}{a^c}\right)\sum_{h=0}^{c-1}\frac{a^h}{h!}\right) \tag{2.24}$$

It is obvious from (3.10b) that $\xi_{ij}^{(k)^*} = 0$ since $\left(T_{ij}^{(k)^*} - t_{ij}^{(k)}\right) > 0$. This leads to the

optimal value of $\nu_{ij}^{(k)^*}$ expressed as:

$$\nu_{ij}^{(k)^*} = \frac{1}{t_{ij}^{(k)}} > 0 \ \forall \ i, j, k \tag{2.25}$$

From the expression (2.22a) and the fact that $\nu_{ij}^{(k)^*} > 0$, we can easily find the optimal solution of $T_{ij}^{(k)^*}$, which is expressed as:

$$T_{ij}^{(k)^*} = t_{ij}^{(k)} + D_{c-k} \ \forall \ i, j, k \tag{2.26}$$

The above expression shows that $T_{ij}^{(k)^*}$ is an exact bound on the actual trip time. It is clear from (2.22b) that $\eta_k^* = 0$ since $\left(\sum_{i=1}^{n} \sum_{\substack{j=1 \\ i \neq j}}^{n} \lambda_i P_{ij}^{(k)^*} - c\mu_k \right) < 0$. Having these parameters defined, the optimal routing proportions $P_{ij}^{(k)*} \ \forall \ i, j, k$ could be found by solving equation (2.24) for $P_{ij}^{(k)^*}$.

2.4 Simulation Results

In this section, we consider a simulation model with 4 PSs and 3 CSs to show the system dynamics and the routing proportions $P_{ij}^{(k)}$ for both the M/M/1 and M/M/c CS models under different parameters. Table 2.2 shows the different values of $t_{ij}^{(k)}$ (time spent on the road only) used in the simulations for all possible routes. These values are generated randomly for the 4 PSs and 3 CSs we have. Uniform destination PS probabilities are assumed from each origin PS (i.e. $q_{ij} = 1/3 \ \forall \ i \neq j$). We consider two types of charging in the simulations, namely battery-swapping and conventional charging. With the conventional charging, we allow the charging rate per charging unit to vary from 8 to 18 EVs/hour. A new study showed that an EV battery fully-depleted could be charged in 5 minutes [31], which corresponds to the value of 12 EVs/hour. Slightly lower (8 to 11 EVs/hour) and higher (13 to 18 EVs/hour) charging rates are also considered to represent cases where the charging stations have low-energy supplies and the EV batteries are not fully-depleted, respectively. For the

Table 2.2: Different values of $t_{ij}^{(k)}$ in hours forall possible routes

$t_{12}^{(1)}$	$t_{12}^{(2)}$	$t_{12}^{(3)}$	$t_{13}^{(1)}$	$t_{13}^{(2)}$	$t_{13}^{(3)}$
0.5	0.7	0.7	0.65	0.5	0.5
$t_{14}^{(1)}$	$t_{14}^{(2)}$	$t_{14}^{(3)}$	$t_{21}^{(1)}$	$t_{21}^{(2)}$	$t_{21}^{(3)}$
0.65	0.6	0.4	0.5	0.7	0.7
$t_{23}^{(1)}$	$t_{23}^{(2)}$	$t_{23}^{(3)}$	$t_{24}^{(1)}$	$t_{24}^{(2)}$	$t_{24}^{(3)}$
0.65	0.4	0.6	0.65	0.5	0.5
$t_{31}^{(1)}$	$t_{31}^{(2)}$	$t_{31}^{(3)}$	$t_{32}^{(1)}$	$t_{32}^{(2)}$	$t_{32}^{(3)}$
0.65	0.5	0.5	0.65	0.4	0.6
$t_{34}^{(1)}$	$t_{34}^{(2)}$	$t_{34}^{(3)}$	$t_{41}^{(1)}$	$t_{41}^{(2)}$	$t_{41}^{(3)}$
0.8	0.3	0.3	0.65	0.6	0.4
$t_{42}^{(1)}$	$t_{42}^{(2)}$	$t_{42}^{(3)}$	$t_{43}^{(1)}$	$t_{43}^{(2)}$	$t_{43}^{(3)}$
0.65	0.5	0.5	0.8	0.3	0.3

battery-swapping option, the charging rate per server varies from 40 to 100 EVs/hour.

Given these charging parameters, the optimal routing proportions $P_{ij}^{(k)}$, $\forall\ i, j, k$ are first illustrated for a wide variety of system variables. The average total trip time and percentage excess charging delay performances achievable by our proposed decision scheme are also tested through extensive simulations, and compared to the conventional shortest time scheme, i.e., the scheme selecting $k^* = \arg\min_k \left\{ t_{ij}^{(k)} \right\}$, and random routing scheme, i.e., the scheme assigning random values to $P_{ij}^{(k)}$ without any optimization (thus emulating a random non-connected driver behavior). Without loss of generality, and to avoid confusion, we will only illustrate the results for PS 1 as an example.

2.4.1 Results for M/M/1 CS Model

In the following figures, the charging stations are assumed to be equipped with battery-swapping technology only, unless otherwise stated. Figure 2.3 shows the behavior of the optimal routing proportions $P_{12}^{(k)}$ as a function of the charging rates μ_1, μ_2 and μ_3, while keeping the departure rate from each of the PSs set to 30 EVs/hour. For this selected origin and destination pair, CS 1 is the one that achieves the shortest time routing. For ease of illustration, we will employ equal charging rates in CSs 2 and 3 (i.e., $\mu_2 = \mu_3$), which enables

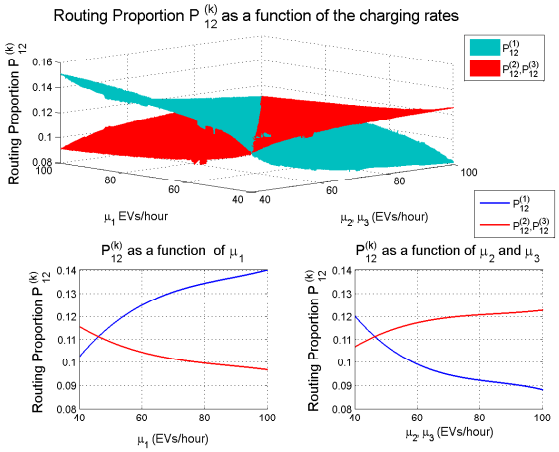

Figure 2.3: Effect of charging rate variation.

varying their common value on one axis of the 3D plot. This setting leads to equal routing proportions variables $P_{12}^{(2)}$ and $P_{12}^{(3)}$, which are illustrated using one curve in Figure 2.3. As shown in the Figure, the proportion $P_{12}^{(1)}$ is lower than $P_{12}^{(2)} = P_{12}^{(3)}$ when the charging rates $\mu_2 = \mu_3$ are comparable to μ_1 even though $(t_{12}^{(1)} < t_{12}^{(2)} = t_{12}^{(3)})$. This occurs due to the optimal balancing of loads on charging stations, which will lead to a smaller average total trip time (as will be illustrated later in Figure 2.5). Even when the charging rate μ_1 is much higher than the other two, the proportion variable $P_{12}^{(1)}$ naturally becomes higher, but non-zero proportions of the EVs are still routed to the other two CSs to minimize the total trip time. The lower left 2D plane in Figure 2.3 represents the plane in the 3D plot having $\mu_2 = \mu_3 = 50$ EVs/hour. As shown, $P_{12}^{(1)}$ increases, whereas $P_{12}^{(2)} = P_{12}^{(3)}$ decrease, as μ_1 increases. On the other hand, the lower right 2D plot represents the plane having $\mu_1 = 50$ EVs/hour. We can see that $P_{12}^{(2)} = P_{12}^{(3)}$ increase, whereas $P_{12}^{(1)}$ decreases, as $\mu_2 = \mu_3$ increase. In both cases, no routing proportion to any CS reaches zero, which means that EVs are still routed to all three CSs.

Figure 2.4 shows how the routing proportions $P_{12}^{(k)}$ behave when varying the departure rate from PS 1 (λ_1), for fixed departure rates from the other PSs and two cases of charging rates at the different CSs. The first case is when the charging rates are set to the following values, $\mu_1 = 70$, $\mu_2 = 90$ and $\mu_2 = 60$ EVs/hour. As shown in the Figure, $P_{12}^{(2)}$ increase while

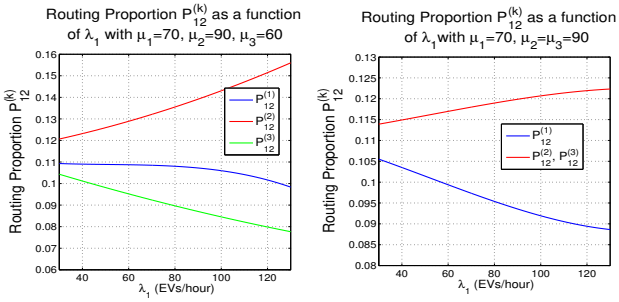

Figure 2.4: Effect of departure rate variations for two cases of charging rate distributions.

$P_{12}^{(3)}$ decreases, despite the fact that $t_{12}^{(2)} = t_{12}^{(3)}$. Even $P_{12}^{(1)}$ is decreasing slowly, despite its smaller trip time without-charging. This shows the effect of the higher charging rate CS (in this example CS 2) in attracting more EVs even when other CSs have equal or even smaller trip times without-charging. The second case is when $\mu_2 = \mu_3 = 90$ EVs/hour and $\mu_1 = 60$ EVs/hour. Again, $P_{12}^{(2)} = P_{12}^{(3)}$ and are both increasing, while $P_{12}^{(1)}$ is decreasing even though it is the shortest time route without charging. Clearly, all these results show the merits of our cloud-based optimization approach in achieving optimal real-time routing proportions, according to real-time values of system parameters, for a better experience for the customers driving these EVs.

Figure 2.5 shows a comparison of the trip and charging temporal behaviors of our proposed optimized scheme with the shortest time route selection and the random routing scheme. The departure rates from PSs 1, 2, 3, and 4 are set to 40, 40, 30, and 30 EVs/hour, respectively, and the charging rates of all CSs are set to 50 EVs/hour. The left sub-figure depicts the comparison of the average total trip time between the three schemes. As shown, the average total trip times of both the shortest time and random routing schemes are higher than that of our proposed optimized scheme for all three destinations PSs 2, 3, and 4. The right sub-figure illustrates the percentage excess duration in the charging stations $\left(\text{defined as } (\tau_{ij}^{(k)} - t_{ij}^{(k)})/t_{ij}^{(k)} \times 100\right)$ by our proposed model in comparison to the conventional shortest time routing scheme. The figure clearly shows the significant reduction achieved by our proposed optimized routing scheme in the percentage excess charging du-

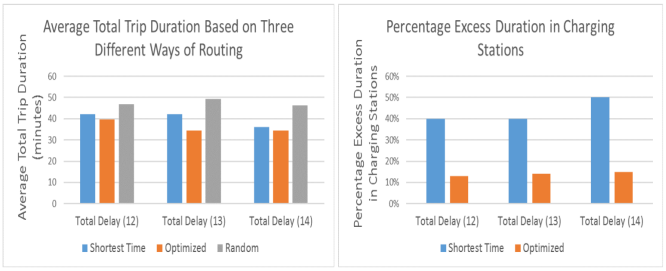

Figure 2.5: Comparison of the trip and charging temporal behaviors of the three tested schemes with battery-swapping technology.

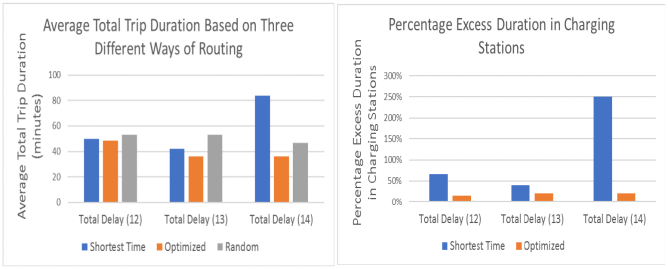

Figure 2.6: Comparison of the trip and charging temporal behaviors of the three tested schemes with conventional charging.

rations, and thus its great impact on reducing the frustration and/or anxiety of customers performing in-route charging of their allocated EVs.

Finally, Figure 2.6 shows the same comparisons of Figure 2.5 for the conventional charging technology (as opposed to battery-swapping in Figure 2.5). The departure rates from PSs 1, 2, 3, and 4 are set to 7, 7, 6, and 6 EVs/hour, respectively, and the charging rates of all CSs are set to 10 EVs/hour. Similar to Figure 2.5, the proposed routing method outperforms the other two methods in the average total trip time performance. Likewise, a tremendous reduction in the excess time spent in CSs can be observed when employing our optimized scheme, which significantly improves the customers' quality of experience.

2.4.2 Results for M/M/c CS Model

In this section, we simulated our model under the same system parameters of the previous section with the charging stations modeled as M/M/c queues. The number of servers (c)

is set to 5 in all the following results. For the following results, the type of charging is the conventional one unless otherwise stated. Figure 2.7 shows the behavior of the optimal routing proportions $P_{12}^{(k)}$ as a function of the charging rates μ_1, μ_2 and μ_3 while keeping the departure rate from each of the PSs set to 30 EVs/hour. The x-axis and y-axis in Figure 2.7 represent the total charging rate in a designated charging stations i.e $c\mu$. The two sub-Figures in Figure 2.7 are two planes of the 3D figure, showing the behavior of the optimal routing proportions $P_{12}^{(k)}$ as a function of the charging rates. In the left sub-figure, the value of μ_2 and μ_3 are set to 10 EVs/hour. Also, μ_1 is set to 10 EVs/hour in the right sub-figure. In all three sub-figures, we can easily notice the same behavior as the one exhibited in the M/M/1 CS models. Likewise, the optimal routing proportions are always non-zero even in extreme cases, which shows the need for and merits of our optimized cloud-based routing approach.

Figure 2.8 shows the behavior of the proportions $P_{12}^{(k)}$ when varying the departure rate from PS 1 (λ_1) while fixing the other the departure rates from the Other PSs to 25 EVs/hour. This setting is tested for two different cases of charging rates. The charging rates are set to $\mu_1 = 14$ EVs/hour, $\mu_2 = 18$ EVs/hour and $\mu_3 = 12$ EVs/hour in the first case. In the other case, the rates are set to the following values $\mu_1 = 14$ EVs/hour and $\mu_2 = \mu_3 = 18$ Evs/hour. The optimal routing proportions $P_{12}^{(k)}$ in Figure 2.8 are behaving in the same way as in Figure 2.4 with small changes in the values, which again gives all credit to our proposed route optimization process.

Figures 2.9 - 2.10 show a comparison between our proposed solution with the shortest time and random routing schemes. In Figure 2.9, the departure rates from PSs 1-4 are set to 40, 40, 30, and 30 EVs/hour, respectively, and the charging rates per charging unit of all CSs are set to 10 EVs/hour (conventional charging). As shown, the proposed method outperforms the other two in both the average total trip time and the excess percentage for charging. Figures 2.10 demonstrates the same comparison with battery-swapping technology at the CSs. In Figure 2.10, the charging rates per charging unit of all CSs are set to 50 EVs/hour

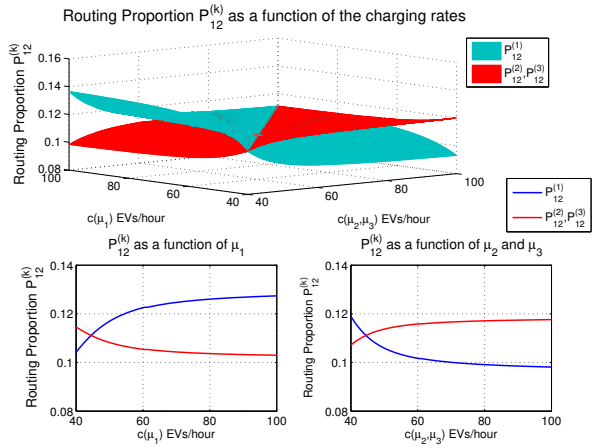

Figure 2.7: Effect of charging rate variation.

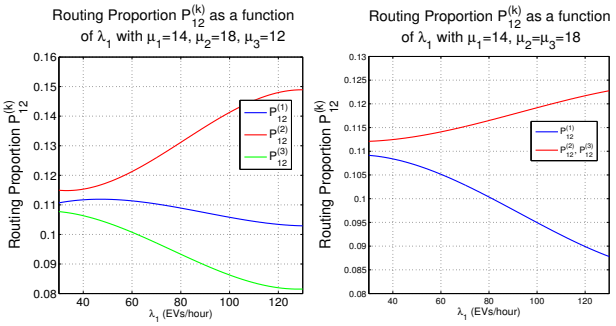

Figure 2.8: Effect of departure rate variations for two cases of charging rate distributions.

and the departure rates from PSs 1-4 are set to 240, 240, 120 and 120 EVs/hour. Figure 2.10 shows that the performance of the proposed routing method is better than the other two schemes in both the average total trip duration and the percentage excess charging durations.

2.4.3 Real-World Scenario

In this section, we present the results of implementing our proposed routing optimization approach with M/M/c CS model for the real-world PSs of Autolib, the well-known current MoD provider in Paris. The different travel times in this study were obtained using Google Maps on January 15, 2018 at 9:05 a.m. [32]. To test our model, we have chosen 10 different Autolib PSs and 3 CSs in Paris [33], all shown in Figure 2.11. The departure rates from PSs

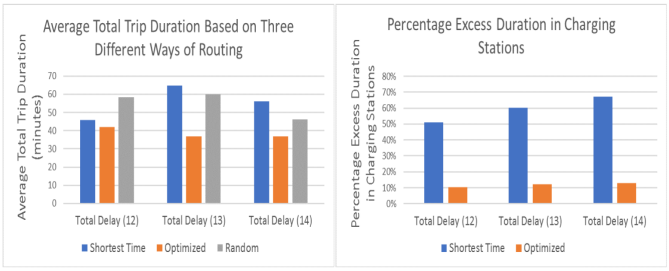

Figure 2.9: Comparison of the trip and charging temporal behaviors of the three tested schemes with conventional charging.

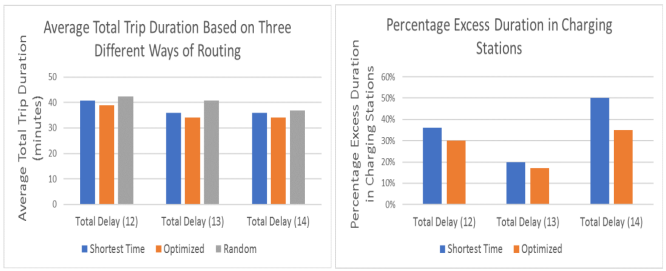

Figure 2.10: Comparison of the trip and charging temporal behaviors of the three tested schemes with battery-swapping technology.

1-10 are set to 7, 9, 8, 7, 8, 8, 8, 8, 8, 12 EVs/hour. The charging rates at all CSs are set to 14 EVs/hour with 2 charging units at each CS (i.e. c=2). Figure 2.12 shows a comparison between our model and the other two schemes of routing for the real-world scenario. Due to space limitations, we limited the comparison to only three destinations. As we can see, the proposed model still outperforms the other two schemes even with a real-world scenario.

2.4.4 Computation Times

Optimization techniques are known to suffer from high execution times due to their nature and the many iterations needed to achieve the optimal solutions. The total number of variables to be calculated in our model is $2 \times n \times (n-1) \times$ m. It is obvious that the execution time will increase as the number of variables and equations increase. The simulations were done using MATLAB 2012 on a computer with i5-core 2.6 GHz Intel processor and 6 Gb RAM [34]. Table 2.3 shows the average execution times and the number of variables for

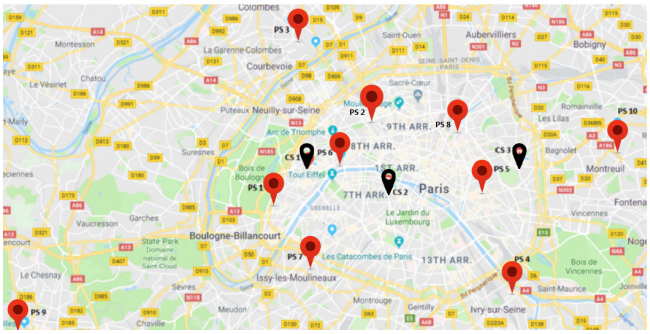

Figure 2.11: Paris map with 10 of Autolib PSs and 3 CSs.

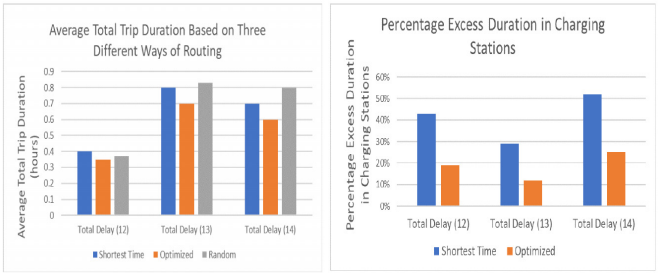

Figure 2.12: Comparison of the trip and charging temporal behaviors of the three tested schemes for real-world scenario.

the three different cases discussed in the simulation results. As we can see, even though the M/M/1 model and M/M/c one have the same number of variables and equations, we see that M/M/c model has higher execution time due to the complexity of the equations in the problem. The real-world example has a higher execution time due to the number of variables and equations. As the number of PSs and CSs increase, the execution time will increase as well. Since the optimal routing proportions are assumed to be calculated in time span of one hour or 30 minutes, the execution time will be within the time span. Figure 2.13 shows a more detailed study on how the computation time is increasing with the number of variables in the M/M/1 model case. As we can see, the time is approximately 55 seconds when the number of variables is 2000 which is still tolerable if the optimization problem has a span of 30 minutes or one hour. In addition, if the simulations were done on C++ rather than MATLAB, it will be 100 times faster which means the proposed methods are highly tolerable even with large number of variables [35].

Table 2.3: Computation times and number of variablesfor all case studies.

	M/M/1 CS Model	**M/M/c CS Model**	**Real-World Scenario**
Total Number of Variables	72	72	540
Execution Time (seconds)	2.85	3.3	11.5

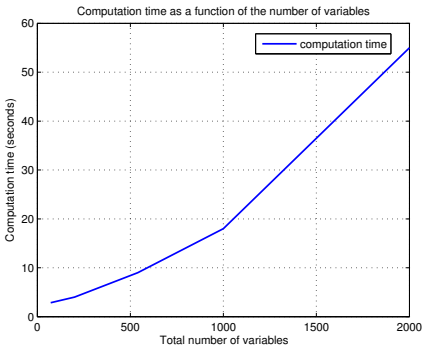

Figure 2.13: Computation time as a function of the total number of variables.

CHAPTER 3

Joint Delay and Cost Optimization of In-Route Charging for MoD-EV Systems

This chapter discusses the issue of the in-route charging similar to Chapter 2 in addition to the cost on charging problem with an objective to minimize the average travel time for all the customers as well as minimizing the charging costs from operator side. The problem is formulated as a dual objective optimization problem using queuing theory based on M/M/1 and M/M/c queues and then solved analytically and numerically to illustrate the performance of the proposed method similar to the previous Chapter.

3.1 System Model

This chapter considers the MoD-EV system in Figure 2.1 similar to Chapter 2, with n passenger stations (PSs) and m charging stations (CSs). As illustrated by the PS queues in Figure 2.1, the model only considers EVs that need charging on the way to the destination by less time-constrained customers. Each charging station is modeled by a queuing system as shown in Figure 2.1. This queuing system can be either an M/M/1 or M/M/c queuing model for all the charging stations in the system. Clearly, the M/M/1 model is a special case of the general M/M/c, and both of them will be considered separately in the analysis. The number of servers c at each CS might be different. From now on, It is labeled by M/M/r_k where r_k is the number of servers at CS k.

Similar to Chapter 2, the overall departure rate of these EVs from PS i is modeled by a Poisson process with rate λ_i EVs / unit time and the probability of a customer to go from origin i to destination j is labeled by q_{ij}. On the other hand, each charging server at CS k can complete either the direct EV charging or the swapping of its battery [11], [18] in an exponentially distributed duration with rate μ_k EVs / unit time per server, which is different from one CS to another given their different supplies of energy. In each CS k, there are two different supplies of energy, namely the renewable and grid sources whose charging rates are

Table 3.1: List of System and Decision Parameters

Parameter	**Definition**
n:	Total number of PSs
m:	Total number of CSs
λ_i:	Departure rate from PS i
q_{ij}:	Probability for customer to go from PS i to PS j
μ_k^r:	Charging or battery-swapping rate at CS k from the renewable energy sources
μ_k^g:	Charging or battery-swapping rate at CS k from the power grid
μ_k:	Total charging rate at CS k
r_k:	The number of servers at CS k
c_k:	cost of charging from the grid at CS k per EV
$t_{ij}^{(k)}$:	Time spent on the road only from PS i to PS j through CS k without considering the charging time
$P_{ij}^{(k)}$:	Decision routing probability to go from PS i to PS j through CS k
$\tau_{ij}^{(k)}$:	Actual trip time from PS i to PS j through CS k including charging
$T_{ij}^{(k)}$:	An upper bound on $\tau_{ij}^{(k)}$

μ_k^r and μ_k^g EVs / unit time per server, respectively, totaling up to μ_k (i.e., $\mu_k^r + \mu_k^g = \mu_k$). As in [8], it is assumed that the costs of charging from the renewable and grid sources are 0 and c_k per EV, respectively. Consequently, EVs will first charge from the renewable energy sources, and will only use the power grid if the arrival rate to the CS is more than μ_k^r (i.e., only if the renewable energy generation rate is not sufficient to cope with the EVs' demand at this CS). Finally, the real-time trip duration, without charging, between PSs i and j through CS k is denoted by $t_{ij}^{(k)}$. Table 3.1 summarizes the different parameters we consider in our model.

Having the operator cloud control collecting all the above time-varying parameters (and thus time-varying of μ_k^r, μ_k^g, c_k and $t_{ij}^{(k)}$ $\forall\, i, j, k$) in real-time due to typical changes in charging and traffic conditions, this controller is required to guide each EV departing from PS i towards PS j to route through and charge in CS k with probability $P_{ij}^{(k)}$ which will lead us to equations (2.1) and (2.2) as in Chapter 2.

The routed EVs from all PSs to CS k queue up to charge, thus acquiring excess delays in these CSs on top of the actual trip time $t_{ij}^{(k)}$ without charging. After departing from the

CS, EVs continue their routes to their destination PSs.

Clearly, the conventional shortest time routing strategy, which routes a customer departing from PS i and destined to PS j through CS $k = \arg\min_k \left\{ t_{ij}^{(k)} \right\}$ may not necessarily be the best strategy since the CS in this route might be overloaded, have insufficient charging rate (especially from the free renewable sources), and/or high cost of charging from the grid, and thus an extremely large (or even unbounded) charging delay or cost. The controller is thus required to periodically determine the optimal routing proportions $P_{ij}^{(k)}$, given the real-time values of λ_i, q_{ij}, μ_k^r, μ_k^g, and $t_{ij}^{(k)}$ $\forall\ i, j, k$, in order to jointly minimize the total trip time of all customers through any route, relative to its $t_{ij}^{(k)}$ value $\forall\ i, j, k$, and the total cost of charging.

Given the system model described above, and well-known thinning properties of Poisson processes, the arrival process to the queue of each CS k is an independent Poisson process with rate λ_k, which can be expressed by equation (3.1) which is obtained in the same way as equation (2.3).

$$\lambda_k = \sum_{\substack{i=1 \\ i \neq j}}^{n} \sum_{j=1}^{n} \lambda_i P_{ij}^{(k)} \tag{3.1}$$

3.2 M/M/1 CS Model

In this section, we will formulate our problem using M/M/1 queues at the different CSs (i.e one charging server per CS). Then, optimal routing decisions will be derived using Lagrangian Analysis and KKT conditions.

3.2.1 Stability Constraints

Since the arrival process to each CS k is Poisson with rate λ_k and the charging duration at each CS k are exponentially distributed with rate μ_k, the overall queuing system at each CS

k becomes an M/M/1 queue [26]. Consequently, the entire system becomes a multi-server queuing system consisting of m independent M/M/1 CS queues with different arrival rates, which depend on the decision probabilities $P_{ij}^{(k)}$, $\forall\ i, j, k$, and different service rates due to their different energy supplies. To ensure the stability of CS k's queue, $\forall k$, the arrival rate to this CS k must be strictly less than its service rate μ_k. That is:

$$\sum_{\substack{i=1 \\ i \neq j}}^{n} \sum_{j=1}^{n} \lambda_i P_{ij}^{(k)} < \mu_k \ = \ \mu_k^r + \mu_k^g \ \forall\ k \tag{3.2}$$

By summing the left hand sides and right hand sides of the inequalities (2.4) for all k, we get the general stability condition of the entire queuing system, expressed as:

$$\sum_{i=1}^{n} \lambda_i \ < \ \sum_{k=1}^{m} \mu_k \ = \ \sum_{k=1}^{m} \left(\mu_k^r + \mu_k^g\right) \tag{3.3}$$

In other words, the sum of the departure rates from all PSs must be strictly less than the sum of all charging rates at all CSs to ensure that the queuing system is stable.

3.2.2 Problem Formulation

From basic analysis of M/M/1 queues [26], the expected charging time (denoted by D_k) at each CS k is expressed as :

$$D_k = \frac{1}{(\mu_k^r + \mu_k^g) - \sum_{\substack{i=1 \\ i \neq j}}^{n} \sum_{j=1}^{n} \lambda_i P_{ij}^{(k)}} \ \forall\ k \tag{3.4}$$

Therefore, the total expected trip time (denoted by $\tau_{ij}^{(k)}$) from PS i to PS j through CS k with in-route charging can be expressed as:

$$\tau_{ij}^{(k)} = t_{ij}^{(k)} + \frac{1}{(\mu_k^r + \mu_k^g) - \sum_{\substack{i=1 \\ i \neq j}}^{n} \sum_{j=1}^{n} \lambda_i P_{ij}^{(k)}} \ \forall\ i, j, k \tag{3.5}$$

Also, the charging cost at CS k can be represented by:

$$Cost_k = c_k \cdot \max\left(0, \sum_{\substack{i=1 \\ i\neq j}}^{n}\sum_{j=1}^{n}\lambda_i P_{ij}^{(k)} - \mu_k^r\right) \ \forall\ k \tag{3.6}$$

As stated earlier, the main objective of our decision probabilities optimization is to jointly minimize both the expected overall trip time for any customer over all routes, relative to their trip time without in-route charging, and the overall cost of charging, while respecting the stability constraint of the system. This problem can be formulated as follows:

$$\begin{aligned}
&\underset{P_{ij}^{(k)}\forall i,j,k}{\text{minimize}} \quad \rho\sum_{\substack{i=1 \\ i\neq j}}^{n}\sum_{j=1}^{n}\sum_{k=1}^{m}\frac{T_{ij}^{(k)}}{t_{ij}^{(k)}} \\
&\qquad + (1-\rho)\sum_{k=1}^{m} c_k \cdot \max\left(0, \sum_{\substack{i=1 \\ i\neq j}}^{n}\sum_{j=1}^{n}\lambda_i P_{ij}^{(k)} - \mu_k^r\right) && \text{(3.7a)} \\
s.t. \quad & t_{ij}^{(k)} + \frac{1}{\mu_k - \sum_{\substack{i=1 \\ i\neq j}}^{n}\sum_{j=1}^{n}\lambda_i P_{ij}^{(k)}} \leq T_{ij}^{(k)} \ \forall\ i,j,k && \text{(3.7b)} \\
& \sum_{k=1}^{m} P_{ij}^{(k)} = q_{ij} \ \forall\ i,j && \text{(3.7c)} \\
& \sum_{\substack{j=1 \\ i\neq j}}^{n}\sum_{k=1}^{m} P_{ij}^{(k)} = 1 \ \forall\ i && \text{(3.7d)} \\
& 0 \leq P_{ij}^{(k)} \ \forall\ i,j,k && \text{(3.7e)} \\
& T_{ij}^{(k)} > t_{ij}^{(k)} \ \forall\ i,j,k && \text{(3.7f)} \\
& \sum_{\substack{i=1 \\ i\neq j}}^{n}\sum_{j=1}^{n}\lambda_i P_{ij}^{(k)} - \mu_k^r < \mu_k^g \ \forall\ k && \text{(3.7g)}
\end{aligned}$$

Constraint (3.7b) with the first objective function guarantee the achievement of the first desired goal (minimizing $\tau_{ij}^{(k)}$ relative to $t_{ij}^{(k)}$) in a weighted epigraph form [27] and the second objective function guarantees the minimization of the total charging costs. Hence, we cast the problem as a weighted sum of these two convex objective functions where $0 \leq \rho \leq 1$.

Constraints (3.7c) and (3.7d) represent the facts on the decisions $P_{ij}^{(k)}$ in (2.1) and (2.2), respectively. Constraint (3.7e) and (3.7c) guarantee that each routing proportion of each source-destination pair EVs is always between 0 and $q_{ij}^{(k)}$, while Constraint (3.7f) guarantees the positivity of the charging delay D_k. Constraint (3.7g) guarantees that the rate of EVs charging from the power grid is less than the charging rate of the grid μ_k^g.

By re-arranging (3.7b), we get:

$$\sum_{\substack{i=1 \\ i \neq j}}^{n} \sum_{j=1}^{n} \lambda_i P_{ij}^{(k)} \leq \mu_k - \frac{1}{T_{ij}^{(k)} - t_{ij}^{(k)}} \; \forall \; i, j, k \tag{3.8}$$

Consequently, the problem in (3.7) becomes a convex optimization problem with convex objective function and convex constraints. Moreover, (3.7f) guarantees the strict positivity of the second term of the right hand side of (3.8), thus making the latter ensure the stability of the system.

3.2.3 Optimal Routing Proportions

Since the problem in (3.7) is convex, it satisfies Slater's theorem. Thus, strong duality holds and the solutions of the primal and dual problems are identical [27]. Furthermore, the Karush-Kuhn-Tucker (KKT) conditions provide necessary and sufficient conditions for optimality [27]. The Lagrangian function corresponding to (3.7) is given in equation (3.9), where $\alpha_{ij}^{(k)}$, $\beta_{ij}^{(k)}$, γ_{ij}, ω_i, $\chi_{ij}^{(k)}$ and η_k are the Lagrange multipliers associated with the different problem constraints. The expressions (3.10) are derived by applying the KKT conditions on

the inequality and equality constraints (3.7b)-(3.7g).

$$L(P,T,\alpha,\beta,\gamma,\omega,\chi,\eta) = \rho\sum_{\substack{i=1\\i\neq j}}^{n}\sum_{j=1}^{n}\sum_{k=1}^{m}\frac{T_{ij}^{(k)}}{t_{ij}^{(k)}} + (1-\rho)\sum_{k=1}^{m}c_k \times \max\left(0, \sum_{\substack{i=1\\i\neq j}}^{n}\sum_{j=1}^{n}\lambda_i P_{ij}^{(k)} - \mu_k^r\right)$$
$$+\sum_{\substack{i=1\\i\neq j}}^{n}\sum_{j=1}^{n}\sum_{k=1}^{m} -\beta_{ij}^{(k)}\left(T_{ij}^{(k)} - t_{ij}^{(k)}\right) + \sum_{\substack{i=1\\i\neq j}}^{n}\sum_{j=1}^{n}\sum_{k=1}^{m}\left(\alpha_{ij}^{(k)}\left(\sum_{\substack{i=1\\i\neq j}}^{n}\sum_{j=1}^{n}\lambda_i P_{ij}^{(k)} + \frac{1}{T_{ij}^{(k)} - t_{ij}^{(k)}} - \left(\mu_k^r + \mu_k^g\right)\right)\right)$$
$$+\sum_{\substack{i=1\\i\neq j}}^{n}\sum_{j=1}^{n}\gamma_{ij}\left(\left(\sum_{k=1}^{m}P_{ij}^{(k)}\right) - q_{ij}\right) + \sum_{\substack{i=1\\i\neq j}}^{n}\sum_{j=1}^{n}\sum_{k=1}^{m}\left(-\chi_{ij}^{(k)}P_{ij}^{(k)}\right)$$
$$+\sum_{\substack{i=1\\i\neq j}}^{n}\omega_i\left(\left(\sum_{j=1}^{n}\sum_{k=1}^{m}P_{ij}^{(k)}\right) - 1\right) + \sum_{k=1}^{m}\eta_k\left(\sum_{\substack{i=1\\i\neq j}}^{n}\sum_{j=1}^{n}\lambda_i P_{ij}^{(k)} - \left(\mu_k^r + \mu_k^g\right)\right) \tag{3.9}$$

The KKT conditions:

$$\alpha_{ij}^{(k)^*}\left(\sum_{\substack{i=1\\i\neq j}}^{n}\sum_{j=1}^{n}\lambda_i P_{ij}^{(k)^*} + \frac{1}{T_{ij}^{(k)^*} - t_{ij}^{(k)}} - \mu_k\right) = 0 \;\forall\; i,j,k \tag{3.10a}$$

$$-\beta_{ij}^{(k)^*}(T_{ij}^{(k)^*} - t_{ij}^{(k)}) = 0 \;\forall\; i,j,k \tag{3.10b}$$

$$\chi_{ij}^{(k)^*}P_{ij}^{(k)^*} = 0 \;\forall\; i,j,k \tag{3.10c}$$

$$\sum_{j=1}^{n}\sum_{k=1}^{m}P_{ij}^{(k)^*} - 1 = 0 \;\forall\; i \tag{3.10d}$$

$$\sum_{k=1}^{m}P_{ij}^{(k)^*} - q_{ij} = 0 \;\forall\; i,j \tag{3.10e}$$

$$\eta_k^*\left(\sum_{\substack{i=1\\i\neq j}}^{n}\sum_{j=1}^{n}\lambda_i P_{ij}^{(k)^*} - (\mu_k^r + \mu_k^g)\right) = 0 \;\forall\; k \tag{3.10f}$$

$$\alpha_{ij}^{(k)^*} \geq 0,\ \beta_{ij}^{(k)^*} \geq 0,\ \zeta_{ij}^{(k)^*} \geq 0,\ \chi_{ij}^{(k)^*} \geq 0,\ \eta_k^* \geq 0 \tag{3.10g}$$

From (3.10), and the fact that the gradient of the Lagrangian function equals 0 at the optimal solution, we obtain the following equations:

$$\frac{\rho}{t_{ij}^{(k)}} - \frac{\alpha_{ij}^{(k)^*}}{\left(T_{ij}^{(k)^*} - t_{ij}^{(k)}\right)^2} - \beta_{ij}^{(k)^*} = 0 \;\forall\; i,j,k \tag{3.11a}$$

$$\lambda_i \left(\sum_{\substack{i=1 \\ i \neq j}}^{n} \sum_{j=1}^{n} \alpha_{ij}^{(k)^*} \right) + \gamma_{ij}^* + \omega_i^* - \chi_{ij}^{(k)^*} + \lambda_i \eta_k^* = 0 \qquad \forall\; i,j,k \qquad \text{if } Cost_k = 0 \tag{3.11b}$$

$$\lambda_i \left(\sum_{\substack{i=1 \\ i \neq j}}^{n} \sum_{j=1}^{n} \alpha_{ij}^{(k)^*} \right) + \gamma_{ij}^* + \omega_i^* - \chi_{ij}^{(k)^*} + \lambda_i \eta_k^* + (1-\rho)\lambda_i c_k = 0 \qquad \forall\; i,j,k \qquad \text{if } Cost_k > 0 \tag{3.11c}$$

It is clear from (3.10b) that $\beta_{ij}^{(k)^*} = 0$, since $\left(T_{ij}^{(k)^*} - t_{ij}^{(k)}\right) > 0$. Also, we can easily see that $\eta_k^* = 0$ from (3.10f). From (3.11a), we get the optimal value of $T_{ij}^{(k)^*}$:

$$T_{ij}^{(k)^*} = \sqrt{\frac{\alpha_{ij}^{(k)^*} t_{ij}^{(k)}}{\rho}} + t_{ij}^{(k)} \;\forall i,j,k \tag{3.12}$$

Multiplying (3.11b) by $P_{ij}^{(k)^*}$, we get for $Cost_k = 0$ that:

$$P_{ij}^{(k)^*} \left(\lambda_i \left(\sum_{\substack{i=1 \\ i \neq j}}^{n} \sum_{j=1}^{n} \alpha_{ij}^{(k)^*} \right) + \gamma_{ij}^* + \omega_i^* - \chi_{ij}^{(k)^*} \right) = 0 \tag{3.13}$$

From equation(3.10c), we can find that $\chi_{ij}^{(k)^*} P_{ij}^{(k)^*} = 0$. $P_{ij}^{(k)^*}$ that is multiplied by γ_{ij}^* and ω_i^* is replaced by $\left(q_{ij} - \sum_{\substack{u=1 \\ u \neq k}}^{m} P_{ij}^{(u)^*} \right)$. Substituting these in (3.13) and rearranging, we

get the optimal routing proportions as:

$$P_{ij}^{(k)^*} = \max \left(0 \ , \ \frac{-\left(q_{ij} - \sum_{\substack{u=1 \\ u \neq k}}^{m} P_{ij}^{(u)^*} \right) \left(\gamma_{ij}^* + \omega_i^* \right)}{\sum_{i=1}^{n} \sum_{j=1}^{n} \alpha_{ij}^{(k)^*}} \right) \qquad (3.14)$$

$$\forall \ i, j, k \text{ if } Cost_k = 0$$

By applying the same procedure done on (3.11b) on (3.11c), we get the optimal routing proportions as in equation (3.15) for $Cost_k > 0$. Note that the second term in equations (3.14) and (3.15) were always found to be positive in all tested scenarios (i.e. simulation results), due to the fact that $\gamma_{ij}^* + \omega_i^*$ is negative and thus makes the value positive. However, we use the form in (3.14) and (3.15) to set the routing proportions to zero in the rare case of having the second term negative.

$$P_{ij}^{(k)^*} = \max \left(0 \ , \ \frac{-\left(q_{ij} - \sum_{\substack{u=1 \\ u \neq k}}^{m} P_{ij}^{(u)^*} \right) \left(\gamma_{ij}^* + \omega_i^* \right)}{\sum_{i=1}^{n} \sum_{j=1}^{n} \alpha_{ij}^{(k)^*} + \lambda_i c_k \left(1 - \rho \right)} \right) \ \forall \ i, j, k \qquad \text{if } Cost_k > 0 \qquad (3.15)$$

3.3 M/M/r_k CS Model

In this section, we will extend the analysis of the special case of queues M/M/1 in the previous section to include the more general form. M/M/r_k are assumed at each CS k with r_k charging servers.

3.3.1 Stability Constraints

Similar to the M/M/1 model explained earlier in Section 3.2, the arrival process to each CS k is again Poisson with rate λ_k as shown in equation (3.1). Here, CS k consists of r_k servers and each server has an exponentially charging rate μ_k. The charging rate μ_k for

each server is the same in each CS and may differ from one CS to another depending on the renewable sources and the power from the gird available at CS k. Consequently, the entire system becomes a multi-server queuing system consisting of m independent CS M/M/r_k queues, with different arrival rates depending on the routing proportions $P_{ij}^{(k)}$, $\forall\ i, j, k$, and different service rates. To ensure the stability of each CS k queue, the arrival rate to this CS k must be strictly less than its total service rate $r_k\mu_k$. That is:

$$\sum_{\substack{i=1 \\ i\neq j}}^{n}\sum_{j=1}^{n}\lambda_i P_{ij}^{(k)} < r_k\mu_k\ \forall\ k \tag{3.16}$$

The general stability condition of the whole queuing system can be found in a similar way to the M/M/1 model from equation (2.16) and is represented by:

$$\sum_{i=1}^{n}\lambda_i\ <\ \sum_{k=1}^{m} r_k\mu_k \tag{3.17}$$

3.3.2 Problem Formulation

From basic analysis of M/M/r_k queues [28], the average charging time (denoted by D_{r_k}) at each CS k can be represented by equation (3.18).

$$D_{r_k} = \frac{1}{(r_k\mu_k - \lambda_k)\left(1 + \left(1 - \frac{\lambda_k}{r_k\mu_k}\right)\left(\frac{r_k!}{(\lambda_k/\mu_k)^{r_k}}\right)\left(\sum_{h=0}^{r_k-1}\frac{(\lambda_k/\mu_k)^h}{h!}\right)\right)} + \frac{1}{\mu_k}\ \forall\ k \tag{3.18}$$

Therefore, the total average trip time $\left(\text{denoted by } \tau_{ij}^{(k)}\right)$ from PS i to PS j through CS k with in-route charging can be represented as:

$$\tau_{ij}^{(k)} = t_{ij}^{(k)} + D_{r_k}\ \forall\ i, j, k \tag{3.19}$$

Also, the charging cost at CS k can be represented in a very similar way to equation (3.6)

by :

$$Cost_k = c_k \cdot \max\left(0, \sum_{\substack{i=1 \\ i\neq j}}^{n}\sum_{j=1}^{n}\lambda_i P_{ij}^{(k)} - r_k\mu_k^r\right) \ \forall\ k \tag{3.20}$$

Given the above expressions and the stability constraints of the system, the problem can be formulated for the M/M/r_k CS model as follows:

$$\begin{aligned} \underset{P_{ij}^{(k)}\forall i,j,k}{\text{minimize}} \quad & \rho\sum_{\substack{i=1 \\ i\neq j}}^{n}\sum_{j=1}^{n}\sum_{k=1}^{m}\frac{T_{ij}^{(k)}}{t_{ij}^{(k)}} \\ & + (1-\rho)\sum_{k=1}^{m} c_k \cdot \max\left(0, \sum_{\substack{i=1 \\ i\neq j}}^{n}\sum_{j=1}^{n}\lambda_i P_{ij}^{(k)} - r_k\mu_k^r\right) \end{aligned} \tag{3.21a}$$

$$s.t. \quad t_{ij}^{(k)} + D_{r_k} \leq T_{ij}^{(k)} \ \forall\ i,j,k \tag{3.21b}$$

$$\sum_{\substack{i=1 \\ i\neq j}}^{n}\sum_{j=1}^{n}\lambda_i P_{ij}^{(k)} < r_k\mu_k \ \forall\ k \tag{3.21c}$$

$$\sum_{k=1}^{m} P_{ij}^{(k)} = q_{ij} \ \forall\ i,j \tag{3.21d}$$

$$\sum_{\substack{j=1 \\ i\neq j}}^{n}\sum_{k=1}^{m} P_{ij}^{(k)} = 1 \ \forall\ i \tag{3.21e}$$

$$0 \leq P_{ij}^{(k)} \ \forall\ i,j,k \tag{3.21f}$$

$$T_{ij}^{(k)} > t_{ij}^{(k)} \ \forall\ i,j,k \tag{3.21g}$$

The formulation is very similar to the M/M/1 CS model. Constraint (3.21b) combined with the objective function guarantee the achievement of the first goal (minimizing the average total trip time relative to the actual time without charging) while the second objective guarantees the minimization of the charging costs. Hence, we formulated the objective function as a weighted sum of the two objectives where $0 \leq \rho \leq 1$. Since the reciprocal of the delay function D_{r_k} is a concave function [29] for constant u_k and r_k, and since the reciprocal of a positive concave function is convex [30], then Constraint (3.21b) is convex. Constraints

(3.21d)-(3.21g) are the same as constraints (3.7f)-(3.7e) in the M/M/1 formulation, and are all linear. Constraints (3.21c) and (3.21g) guarantee the stability of the queuing system and are also all linear. In addition, constraint (3.21c) guarantees that number of EVs that will charge from the grid is less than the charging rate of the grid μ_k^g at CS k. Consequently, the problem in (3.21) is a convex optimization problem with convex objective function and convex constraints.

3.3.3 Optimal Routing Proportions

Similar to the M/M/1 analysis in Section 3.2.3, since the problem (3.21) is convex and satisfies Slater's conditions then a strong duality holds. That means the solutions of the primal and and dual problems are identical, and the KKT conditions provide necessary and sufficient conditions for optimality [27]. The Lagrangian function for the problem in (3.21) is given by Equation (3.22), where $\nu_{ij}^{(k)}$, ζ_k, $\xi_{ij}^{(k)}$, κ_{ij}, σ_i, and $\psi_{ij}^{(k)}$ are the Lagrange multiplies for the different constraints in (3.21). In addition, the expressions (3.23) are obtained by applying the KKT conditions on the optimization problem in (3.21).

$$
\begin{aligned}
L(P,T,\nu,\zeta,\xi,\kappa,\psi,\sigma) &= \rho \sum_{\substack{i=1\\ i\neq j}}^{n}\sum_{j=1}^{n}\sum_{k=1}^{m}\frac{T_{ij}^{(k)}}{t_{ij}^{(k)}} + (1-\rho)\sum_{k=1}^{m} c_k \times \max\left(0, \sum_{\substack{i=1\\ i\neq j}}^{n}\sum_{j=1}^{n}\lambda_i P_{ij}^{(k)} - r_k\mu_k^r\right) \\
&+ \sum_{\substack{i=1\\ i\neq j}}^{n}\sum_{j=1}^{n}\sum_{k=1}^{m}\left(\nu_{ij}^{(k)}\left(\sum_{\substack{i=1\\ i\neq j}}^{n}\sum_{j=1}^{n} t_{ij}^{(k)} + D_{r_k} - T_{ij}^{(k)}\right)\right) + \sum_{k=1}^{m}\left(\zeta_k \sum_{\substack{i=1\\ i\neq j}}^{n}\sum_{j=1}^{n}\lambda_i P_{ij}^{(k)} - r_k\mu_k\right) \\
&+ \sum_{\substack{i=1\\ i\neq j}}^{n}\sum_{j=1}^{n}\sum_{k=1}^{m} -\xi_{ij}^{(k)}\left(T_{ij}^{(k)} - t_{ij}^{(k)}\right) + \sum_{\substack{i=1\\ i\neq j}}^{n}\sum_{j=1}^{n}\kappa_{ij}\left(\left(\sum_{k=1}^{m} P_{ij}^{(k)}\right) - q_{ij}\right) \\
&+ \sum_{\substack{i=1\\ i\neq j}}^{n}\sum_{j=1}^{n}\sum_{k=1}^{m}\left(-\psi_{ij}^{(k)} P_{ij}^{(k)}\right) + \sum_{\substack{i=1\\ i\neq j}}^{n}\sigma_i\left(\left(\sum_{j=1}^{n}\sum_{k=1}^{m} P_{ij}^{(k)}\right) - 1\right)
\end{aligned}
\tag{3.22}
$$

The KKT conditions:

$$\nu_{ij}^{(k)^*}\left(t_{ij}^{(k)} + D_{r_k} - T_{ij}^{(k)^*}\right) = 0 \;\forall\; i,j,k \tag{3.23a}$$

$$\zeta_k^*\left(\sum_{\substack{i=1\\ i\neq j}}^{n}\sum_{j=1}^{n}\lambda_i P_{ij}^{(k)^*} - r_k\mu_k\right) = 0 \;\forall\; k \tag{3.23b}$$

$$-\xi_{ij}^{(k)^*}\left(T_{ij}^{(k)^*} - t_{ij}^{(k)}\right) = 0 \;\forall\; i,j,k \tag{3.23c}$$

$$\psi_{ij}^{(k)^*} P_{ij}^{(k)^*} = 0 \;\forall\; i,j,k \tag{3.23d}$$

$$\sum_{j=1}^{n}\sum_{k=1}^{m} P_{ij}^{(k)^*} - 1 = 0 \;\forall\; i \tag{3.23e}$$

$$\sum_{k=1}^{m} P_{ij}^{(k)^*} - q_{ij} = 0 \;\forall\; i,j \tag{3.23f}$$

$$\nu_{ij}^{(k)^*} \geq 0,\; \zeta_k^* \geq 0,\; \xi_{ij}^{(k)^*} \geq 0,\; \psi_{ij}^{(k)^*} \geq 0 \tag{3.23g}$$

From (3.23) and the fact the gradient of the Lagrangian function equals 0 at the optimal solutions, we obtain equations (3.24), (3.25) and (3.26).

$$\frac{\rho}{t_{ij}^{(k)}} - \nu_{ij}^{(k)^*} - \xi_{ij}^{(k)^*} = 0 \;\forall\; i,j,k \tag{3.24}$$

$$\kappa_{ij}^* - \psi_{ij}^{(k)^*} + \sigma_i^* + \left(\sum_{\substack{i=1\\ i\neq j}}^{n}\sum_{j=1}^{n}\nu_{ij}^{(k)^*}\right) \times \left(\frac{\lambda_i q - (r_k\mu_k - \lambda_k)\left(\frac{-\lambda_i}{r_k\mu_k}\left(\frac{r_k!}{a^{r_k}}\right)\Sigma_{h=0}^{r_k-1}\left(\frac{a^h}{h!}\right) - \frac{r_k\lambda_i}{\mu_k}\frac{r_k!}{a^{r_k+1}}\left(1-\frac{a}{r_k}\right)\Sigma_{h=0}^{r_k-1}\left(\frac{a^h}{h!}\right) + \frac{\lambda_i}{\mu_k}\left(1-\frac{a}{r_k}\right)\left(\frac{r_k!}{a^{r_k}}\right)\Sigma_{h=1}^{r_k-1}\left(\frac{a^h}{h!}\right)\right)}{q^2}\right) = 0$$

$$if\ Cost_k = 0\ \ where\ \lambda_k = \sum_{\substack{i=1\\ i\neq j}}^{n}\sum_{j=1}^{n}\lambda_i P_{ij}^{(k)^*}\ ,\ a = \frac{\lambda_k}{\mu_k}\ and\ q = \left(r_k\mu_k - \lambda_k\right)\left(1 + \left(1-\frac{a}{r_k}\right)\left(\frac{r_k!}{a^{r_k}}\right)\sum_{h=0}^{r_k-1}\frac{a^h}{h!}\right) \tag{3.25}$$

It is easy to see from (3.23c) that $\xi_{ij}^{(k)^*} = 0$ since $\left(T_{ij}^{(k)^*} - t_{ij}^{(k)}\right) > 0$. This leads to the

$$(1-\rho)\lambda_i c_k + \kappa_{ij}^* - \psi_{ij}^{(k)^*} + \sigma_i^* + \left(\sum_{\substack{i=1 \\ i\neq j}}^{n}\sum_{j=1}^{n}\nu_{ij}^{(k)^*}\right) \times$$

$$\left(\frac{\lambda_i q - (r_k\mu_k - \lambda_k)\left(\frac{-\lambda_i}{r_k\mu_k}\left(\frac{r_k!}{a^{r_k}}\right)\sum_{h=0}^{r_k-1}\left(\frac{a^h}{h!}\right) - \frac{r_k\lambda_i}{\mu_k}\frac{r_k!}{a^{r_k+1}}\left(1-\frac{a}{r_k}\right)\sum_{h=0}^{r_k-1}\left(\frac{a^h}{h!}\right) + \frac{\lambda_i}{\mu_k}\left(1-\frac{a}{r_k}\right)\left(\frac{r_k!}{a^{r_k}}\right)\sum_{h=1}^{r_k-1}\left(\frac{a^h}{h!}\right)\right)}{q^2}\right) = 0$$

$$if\ Cost_k > 0\ where\ \lambda_k = \sum_{\substack{i=1 \\ i\neq j}}^{n}\sum_{j=1}^{n}\lambda_i P_{ij}^{(k)^*}\ ,\ a = \frac{\lambda_k}{\mu_k}\ and\ q = \left(r_k\mu_k - \lambda_k\right)\left(1 + \left(1-\frac{a}{r_k}\right)\left(\frac{r_k!}{a^{r_k}}\right)\sum_{h=0}^{r_k-1}\frac{a^h}{h!}\right) \quad (3.26)$$

value of optimal value of $\nu_{ij}^{(k)}$ expressed as:

$$\nu_{ij}^{(k)^*} = \frac{\rho}{t_{ij}^{(k)}} > 0\ \forall\ i,j,k \quad (3.27)$$

From the expression (3.23a) and the fact that $\nu_{ij}^{(k)^*} > 0$, we can easily find the optimal solution of $T_{ij}^{(k)^*}$, which is expressed as:

$$T_{ij}^{(k)^*} = t_{ij}^{(k)} + D_{r_k}\ \forall\ i,j,k \quad (3.28)$$

The above expression shows that $T_{ij}^{(k)^*}$ is an exact bound on the actual trip time. It is clear from (3.23b) that $\zeta_k^* = 0$ since $\left(\sum_{i=1}^{n}\sum_{\substack{j=1 \\ i\neq j}}^{n}\lambda_i P_{ij}^{(k)^*} - r_k\mu_k\right) < 0$. Having these parameters defined, the optimal routing proportions $P_{ij}^{(k)*}\ \forall\ i,j,k$ could be found by solving equations (3.25) and (3.26) for $P_{ij}^{(k)^*}$ for the cases of $Cost_k = 0$ and $Cost_k > 0$, respectively.

3.4 Simulation Results

In this section, we consider a simulation model with 4 PSs and 3 CSs as in Section 2.4 to evaluate the performance of our proposed model for both types of queues at CSs M/M/1 and M/M/r_k. Table 2.2 shows the different values of $t_{ij}^{(k)}$ (time spent on the road only) used in the simulations for all possible routes. Uniform destination PS probabilities are assumed from each source PS (i.e. $q_{ij} = 1/3\ \forall\ i \neq j$). Although our model works for all types of charging,

conventional charging is used to show the performance of our proposed model when having to charge the EV from the power grid when renewable energy sources are exhausted. We allow the total charging rate (μ_k) per server at CS k to vary from 8 to 28 EVs/hour. A new study showed that an EV battery fully-depleted could be charged in 5 minutes [31], which corresponds to the value of 12 EVs/hour. Slightly lower (8 to 11 EVs/hour) and higher (13 to 28 EVs/hour) charging rates are also considered to represent cases where the charging stations have low-energy supplies (or longer than 5 minutes charging time) and customers not fully charging the batteries to reduce their delays, respectively.

Given this setting for the charging rates, the optimal routing proportions $P_{ij}^{(k)}, \forall\, i, j, k$ are first illustrated for a wide variety and interplay of system variables. The average total trip time, percentage excess charging delay, and total charging cost performances achievable by our proposed decision scheme are also tested through extensive simulations, and compared to the conventional shortest time scheme, i.e., the scheme selecting $k^* = \arg\min_k \left\{ t_{ij}^{(k)} \right\}$, and random routing scheme, i.e., the scheme assigning random values to $P_{ij}^{(k)}$ without any optimization (thus emulating a random non-connected driver behavior). Due to space limitation, we will only illustrate the results for PS 1 as an example. In most of the following simulations, the value of ρ is chosen to be either 0.25 or 0.5.

3.4.1 Results for M/M/1 CS Model

Figure 3.1 illustrates the behavior of the routing proportions $P_{12}^{(k)}$ as a function of the renewable sources' charging rates μ_1^r, μ_2^r and μ_3^r, while the departure rates from the PSs are set to 20, 15, 15 and 15 EVs/hour respectively. The maximum charging rate from the grid (i.e., $\mu_k^g\ \forall k$) is set to 10 EVs/hour in all CSs, while the charging costs from the grid are set to $c_1 = 2$ and $c_2 = c_3 = 1$ cost unit/EV. Also, ρ is chosen to be 0.5. For ease of illustration, Table 2.2 shows equal without-charging trip times from PS 1 to PS 2 through both CSs 2 and 3, which is larger than the time through CS 1 (i.e., $t_{12}^{(2)} = t_{12}^{(3)} > t_{12}^{(1)}$). We will also assume

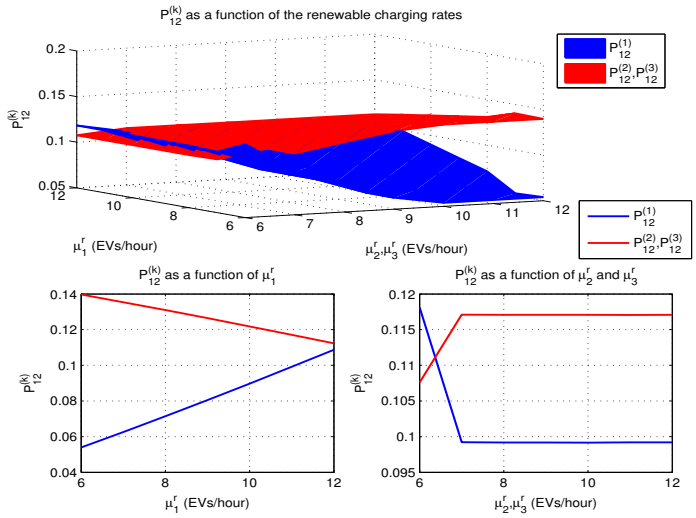

Figure 3.1: Effect of renewable charging rate variation.

equal charging rates in CSs 2 and 3 (i.e., $\mu_2 = \mu_3$), which enables varying their common value on one axis of the 3D plot. This setting leads to equal routing proportions $P_{12}^{(2)}$ and $P_{12}^{(3)}$, which are illustrated using one curve in Figure 3.1. As shown in the figure, $P_{12}^{(1)}$ is lower than $P_{12}^{(2)} = P_{12}^{(3)}$ when the charging rates $\mu_2^r = \mu_3^r$ are much higher than μ_1^r since the delay of charging and the cost are less in CSs 2 and 3 even though $(t_{12}^{(1)} < t_{12}^{(2)} = t_{12}^{(3)})$. Even when the charging rate μ_1^r becomes much higher than the other two, $P_{12}^{(1)}$ starts to increase but is still less than the other two, since the cost of charging in CS 1 is double that of the other two CSs. The lower left 2D plane in Figure 3.1 represents the plane in the 3D plot having $\mu_2^r = \mu_3^r = 10$ EVs/hour. As shown, $P_{12}^{(1)}$ increases as μ_1^r increases, while being still lower than $P_{12}^{(2)} = P_{12}^{(3)}$ (which gradually decrease, as μ_1^r increases) due to the charging cost. On the other hand, the lower right 2D plot represents the plane having $\mu_1^r = 10$ EVs/hour. We can see that $P_{12}^{(2)} = P_{12}^{(3)}$ increase then saturate, whereas $P_{12}^{(1)}$ decreases then saturates, as $\mu_2^r = \mu_3^r$ increase. We see that $P_{12}^{(2)} = P_{12}^{(3)}$ increase and $P_{12}^{(1)}$ decreases at the beginning (i.e., at low charging rates at CS s2 and 3) due to their lower charging costs from the grid. As the renewable charging rates surpass a certain value, accessing grid charging becomes very minimal and unnecessary at all stations, which stabilizes the proportions to the values minimizing the delays.

Figure 3.2 illustrates how the routing proportions $P_{12}^{(k)}$ behave when varying the departure rate from PS 1 (λ_1), for fixed departure rates from other PSs, different/fixed renewable/grid charging rates, and two cases of charging costs at the different CSs. The charging rates from renewable sources are set to $\mu_1^r = 10$, $\mu_2^r = 12$ and $\mu_3 = 18$ EVs/hour, and the fixed charging rate from the grid (i.e., $\mu_1^g = \mu_2^g = \mu_3^g$) is set to 10 EVs/hour. ρ is set to 0.25 in this simulation. The first case is when the charging costs are set equal to $c_1 = c_2 = c_3 = 1$ cost unit/EV, which is illustrated in the left plot. As λ_1 increases in the low range, $P_{12}^{(3)}$ increases while $P_{12}^{(1)}$ decreases and $P_{12}^{(2)}$ remains fairly constant. This occurs since CS 3 has a higher rate of renewable energy, which makes it the most attractive from the delay and the cost (almost all its EVs charge from the renewable source) perspectives. As λ_1 grows to higher ranges, the load on CS 3 becomes high enough to mandate charging from the grid, thus reducing its attractiveness (and thus reducing $P_{12}^{(3)}$) as opposed to CS 1 (and thus $P_{12}^{(1)}$ increases). However, CS 3 still gets the higher share due to its higher renewable and overall charging rates, thus resulting in less delays and less EVs charging from the grid. The second case is when $c_1 = c_2 = 1$ and $c_3 = 1.5$ cost unit/EV, which is illustrated in the right plot of Figure 3.2. Again, at lower ranges of increasing λ_1, $P_{12}^{(3)}$ is increasing. Due to the same effect depicted for the same range in the left plot. As λ_1 grows to the intermediate range, forcing all CSs to need grid charging, the higher cost in c_3 compared to c_1 and c_2 results in a steeper drop (compared to the left plot) in $P_{12}^{(3)}$ to even below the proportions of the other two CSs. However, as λ_1 grows very large, the cost of charging becomes less of an issue compared to the delays, which gives a boost (drop) again to $P_{12}^{(3)}$ ($P_{12}^{(1)}$ and $P_{12}^{(2)}$) as it has higher (lower) charging rates. All these variations clearly demonstrate the merits of our cloud-enabled optimization approach due to the high sensitivity of the system behavior (delay and cost wise) to the real-time values of all the above parameters.

Figure 3.3 shows how the routing proportions $P_{12}^{(k)}$ vary as a function of the charging costs c_k. The departure rates from all PSs are set to 17 EVs/hour while the renewable energy charging rates are set as follow $\mu_1^r = 10$ EVs/hour and $\mu_2^r = \mu_3^r = 16$ EVs/hour. The

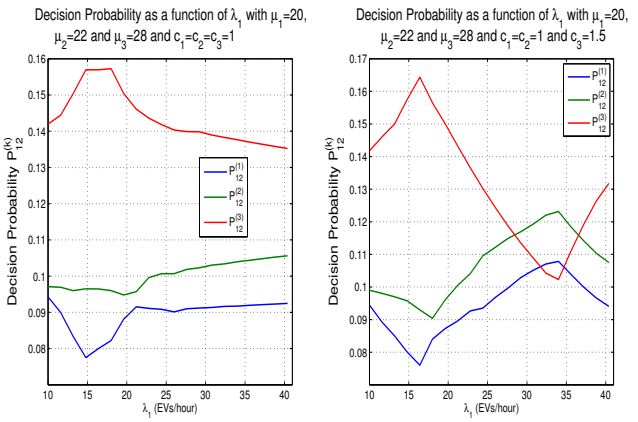

Figure 3.2: Effect of departure rate variations for two cases of charging rate distributions.

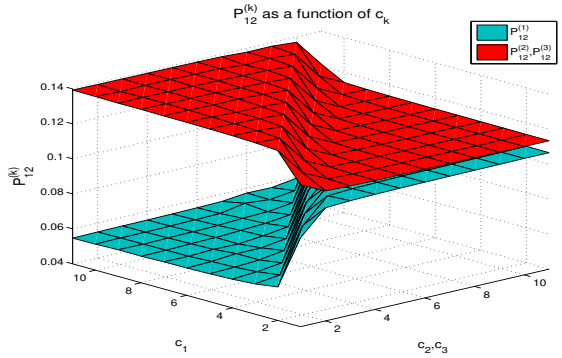

Figure 3.3: Effect of varying the charging prices.

charging rates from the grid are set to 10 EVs/hour in all CSs. The value of ρ here is set 0.5. Similar to Figure 2.3, $P_{12}^{(1)}$ is shown in one curve while the other one illustrates the behavior of $P_{12}^{(2)} = P_{12}^{(3)}$ since CSs 2 and 3 have the same settings and $t_{12}^{(2)} = t_{12}^{(3)}$. As shown in the figure, the proportions $P_{12}^{(2)} = P_{12}^{(3)}$ are much higher than $P_{12}^{(1)}$ when the cost at CS 1 c_1 is high compared to the other two. Even when c_2 and c_3 are much higher than c_1, the proportions $P_{12}^{(2)} = P_{12}^{(3)}$ are still slightly higher than $P_{12}^{(1)}$ due to their higher charging rates.

Figure 3.4 shows the trade-off between the two problem objectives (i.e., total cost and the average ratio of trip times with and without charging) as a function of ρ (varying from 0.05 to 0.95). The departure rates form all PSs are set to 14 EVs/hour and the renewable charging rates are set as follow $\mu_1^r = \mu_2^r = 10$ EVs/hour and $\mu_3^r = 14$ EVs/hour. The grid

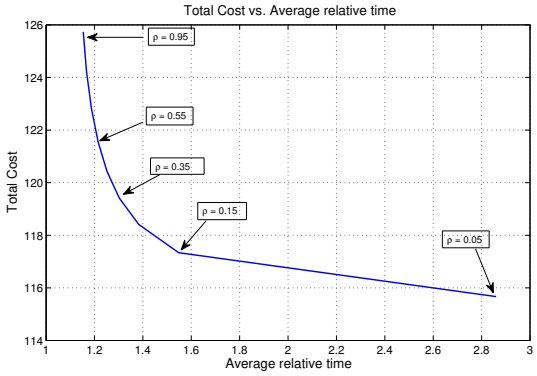

Figure 3.4: Total cost vs. Average relative time for different values of ρ.

charging rate at all CSs is set to 10 EVs/hour and the charging costs are set to the following values $c_1 = c_2 = 1$ and $c_3 = 1.5$ cost unit/EV. On one end of the curve, the highest value of $\rho = 0.95$ gives the highest total cost and the lowest total delay. On the other end, the lowest value of $\rho = 0.05$ gives the lowest total cost and the highest delay for this specific configuration. The figure can be indeed used to determine the best choice of ρ to achieve a certain upper bound constraint on either or both metrics. For example, for this particular configuration, if the trip time ratio (cost) is not to exceed 1.6 (120 cost units/hour),ρ must be chosen to be 0.15 (0.35) to achieve the lowest cost (trip time ratio) while satisfying the above trip time ratio (cost) constraint.

Finally, Figures 3.5 and 3.6 compare our proposed optimized scheme with the shortest time path selection and the random routing scheme in terms of the total with-charging trip duration and charging cost. The departure rates from PSs 1, 2, 3, and 4 are set to 18, 18, 14, and 14 EVs/hour, respectively, the renewable charging rates of all CSs are set to 10 EVs/hour, the grid charging rates of all CSs are set to 12 EVs/hour and the cost of charging are set 15, 10 and 12 cost unit/EV, respectively. Here, the value of ρ is set to 0.5. Figure 2.5 depicts the comparison of the average total trip time achieved by the three schemes. As shown, the average total trip time in the shortest time and random schemes is higher than that of our proposed optimized scheme for all three destinations PSs 2, 3, and 4. Figure

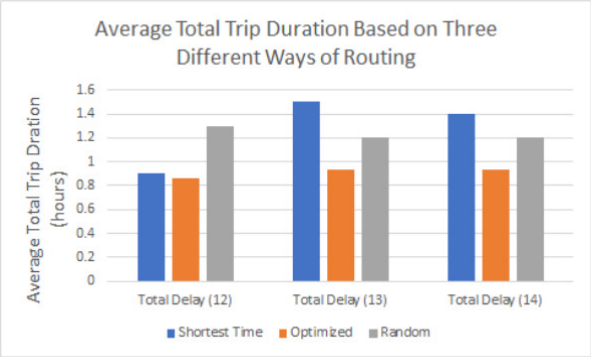

Figure 3.5: Comparison of the total trip time of the three tested schemes.

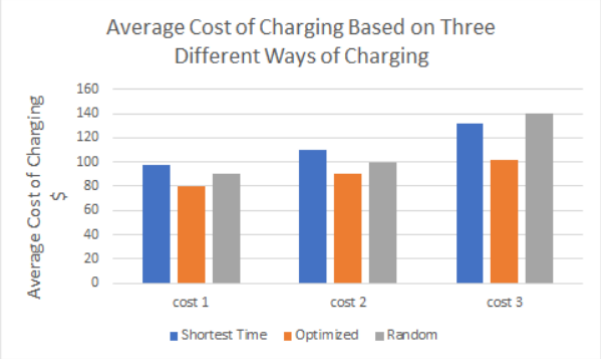

Figure 3.6: Comparison of the charging costs of the three tested schemes.

2.6 shows that our proposed method also outperforms the other two in terms of total cost. Consequently, tremendous gains to both the customers and the operator can be observed when employing our optimized scheme.

3.4.2 Results for M/M/r_k CS Model

In this section, we simulated the system under the same model with 4 PSs and 3 CSs. The CS model is M/M/r_k queues. Similar to Figure 2.3, Figure 3.7 shows the behavior of the optimal routing decisions $P_{12}^{(k)}$ with variation of the renewable charging rates. The x-axis and y-axis in the Figure represent the charging rate per server. The departure rates from all PSs are set to 26 EVs/hour. CSs 2 and 3 have the same settings to allow varying $P_{12}^{(2)}$ and $P_{12}^{(3)}$ on one axis similar to Figure 3.1. The charging rates from the grid are set to 10

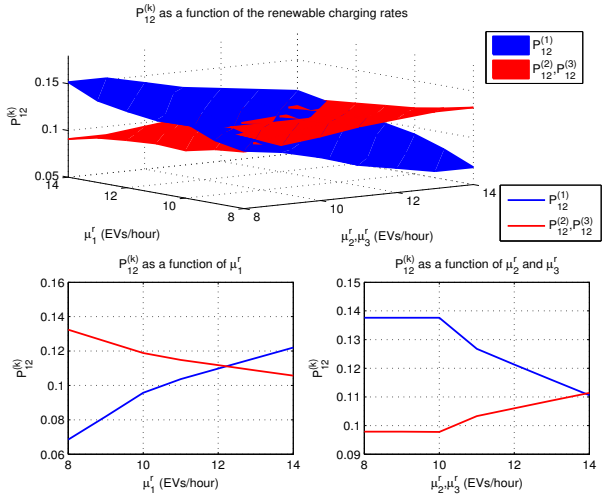

Figure 3.7: Effect of renewable charging rate variation.

EVs/hour while the number of servers at each CS is set to 2 (i.e $\mu_k^g = 10$ and $r_k = 2\ \forall k$). The charging costs from the grid are set as follows $c_1 = 2$ and $c_2 = c_3 = 1$ cost unit/EV, and $\rho = 0.5$. The two sub-Figures are two planes taken from the 3D one. The left sub-figure is when $\mu_2^r = \mu_3^r = 13$ EVs/hour while the right sub-figure is with $\mu_1^r = 13$ EVs/hour. The curves show very similar behavior to Figure 3.1 in M/M/1 CS model. The routing decisions $P_{12}^{(k)}$ have slightly different values from the ones in Figure 3.1 but still having the same general behavior which shows the merit of our proposed method. Figure 3.8 shows how the routing decisions $P_{12}^{(k)}$ behave when varying the departure rate from PS 1 (λ_1), for fixed departure rates from other PSs, fixed renewable/grid charging rates, and two cases of charging costs at the different CSs. The charging rates from renewable sources are set to $\mu_1^r = 10$, $\mu_2^r = 12$ and $\mu_3 = 14$ EVs/hour, and the fixed charging rate from the grid is set to 10 EVs/hour. ρ is set to 0.25 in this simulation. The number of server at CSs are set to $r_1 = 3$ and $r_2 = r_3 = 2$ servers. Similar to Figure 3.2, the first case is when the charging costs are set equal to $c_1 = c_2 = c_3 = 1$ cost unit/EV, which is illustrated in the left plot. As λ_1 increases in the low range, $P_{12}^{(1)}$ decreases while $P_{12}^{(2)}$ and $P_{12}^{(3)}$. As we can see, $P_{12}^{(1)}$ has the higher value at the beginning since CS 1 has the higher rate but as the arrival rate λ_1 increases $P_{12}^{(1)}$ decreases while the other two are increasing to both minimize the delay and

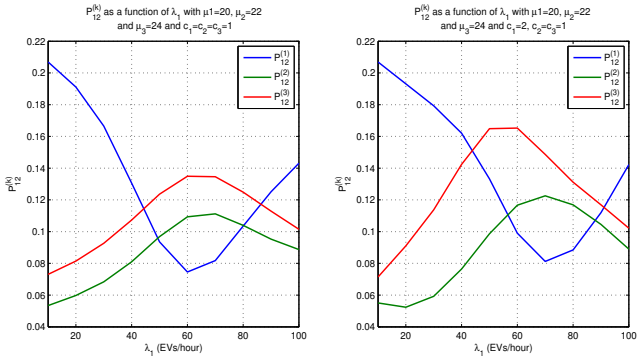

Figure 3.8: Effect of departure rate variations for two cases of charging cost distributions.

the cost. However, this behavior changes at the middle since now all EVs have to charge from the grid. $P_{12}^{(1)}$ is increasing now while the other two are decreasing since it is attractive from both the cost and delay point of view.

The second case is when $c_1 = 1.5$ and $c_2 = c_3 = 1$ cost unit/EV, which is illustrated in the right plot of Figure 3.8. The plot has very similar behavior to the left sub-figure. $P_{12}^{(1)}$ decreases while the other two decisions are increasing in the first part of the curve since the arrival rate increasing. However, $P_{12}^{(2)}$ and $P_{12}^{(3)}$ are increasing much faster than the left sub-figure. Again, the behavior of the decisions change in the middle of the plot when all of them need to charge from the grid. As we can see, $P_{12}^{(1)}$ is increasing while the other two are decreasing even though the cost of CS 1 is higher but it is much better in term of delay compared to CS 2 and 3 which shows how the optimization problem is sensitive to the parameters.

Figure 3.9 shows how the routing decisions $P_{12}^{(k)}$ behave when varying the cost of charging from the grid while keeping all the parameters constants. The departure rates from all PSs are set to 15 EVs/hour while the charging rates from the grid are set to 10 EVs/hour. The charging rates from the renewable sources are set as follows $\mu_1^r = 10$ and $\mu_2^r = \mu_3^r = 12$ EVs/hour. Two charging servers are installed at each CS. The decisions are behaving in a very similar way to Figure 3.3. $P_{12}^{(1)}$ is shown in one curve while the other one illustrates the behavior of $P_{12}^{(2)} = P_{12}^{(3)}$ since CSs 2 and 3 have the same settings and $t_{12}^{(2)} = t_{12}^{(3)}$. As shown in

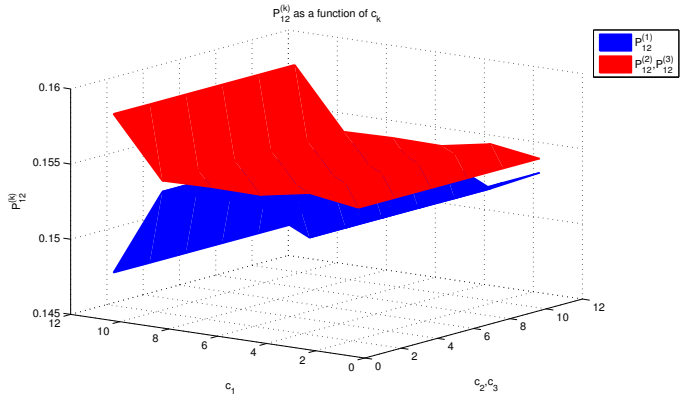

Figure 3.9: Effect of varying the charging prices.

the figure, the proportions $P_{12}^{(2)} = P_{12}^{(3)}$ are higher than $P_{12}^{(1)}$ when the cost at CS 1 c_1 is high compared to the other two. Even when c_2 and c_3 are much higher than c_1, the proportions $P_{12}^{(2)} = P_{12}^{(3)}$ are still slightly higher than $P_{12}^{(1)}$ due to their higher charging rates.

Figure 3.10 shows the trade-off between the two objectives (i.e total Cost and average relative time) for the case of M/M/r_k at CSs as a function of ρ where ρ varied from 0.05 to 0.95 in the simulation. The departure rates from all PSs are set to 40 EVs/hour while the number of servers at each CS is set as as follows $r_1 = 2$ and $r_2 = r_3 = 3$ servers. The charging rates from the grid are set to 10 EVs/hour and the charging from renewable sources are set to the following values $u_1^r = u_2^r = 10$ and $u_3^r = 12$ EVs/hour. The cost of charging from the grid are set to $c_1 = c_2 = 1$ and $c_3 = 2$ cost unit/EV. The Figure has the same general shape of Figure 3.4 but with different values. As we can see in the Figure, $\rho = 0.95$ gives the lowest average relative time and the highest total cost while the opposite case is observed when $\rho = 0.05$ for this setting of the parameters. The Figure can be used to choose the best value of ρ depending on the customer and operator restriction on both the delay and the cost, respectively. In this Figure, choosing ρ to be between 0.65 and 0.25 gives acceptable values on both objectives.

Figures 3.11 and 3.12 compare the performance of our proposed method with two other

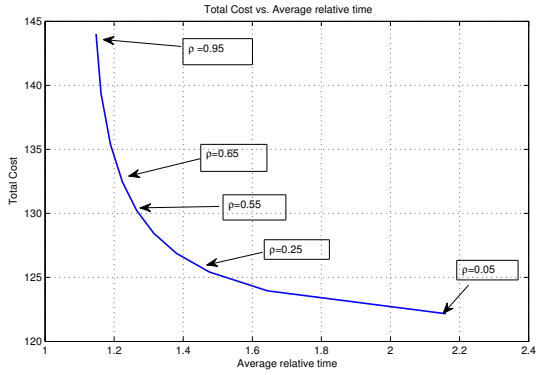

Figure 3.10: Total cost vs. Average relative time for different values of ρ.

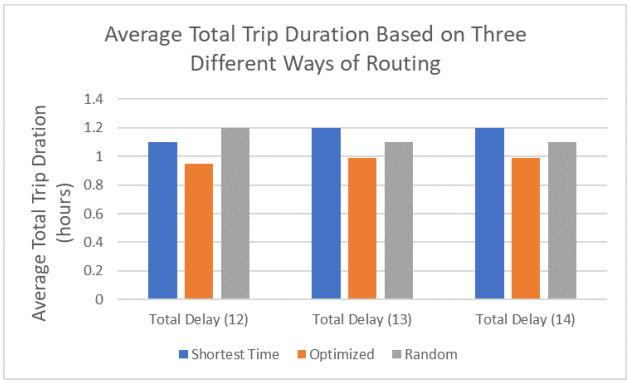

Figure 3.11: Comparison of the total trip time of the three tested schemes.

schemes of routing, shortest time and random routing decisions for both the average delay and total cost. Both Figures are tested under the same system parameters. The departure rates from all PSs are set 28 EVs/hour. The charging rates from the grid are set to 10 EVs/hour at all CSs while charging rates from the renewable sources are set to $\mu_1^r = \mu_2^r = 10$ and $\mu_3^r = 12$ EVs/hour. Two servers are installed at each CS (i.e $r_k = 2\ \forall k$). The cost of charging from the grid is set to $c_1 = 7$, $c_2 = 8$ and $c_3 = 10$ cost unit/EV. As observed in both Figures, our proposed method outperforms the other two methods of routing in both the average delay and the total cost which the merits of our proposed method for both the customers and operator.

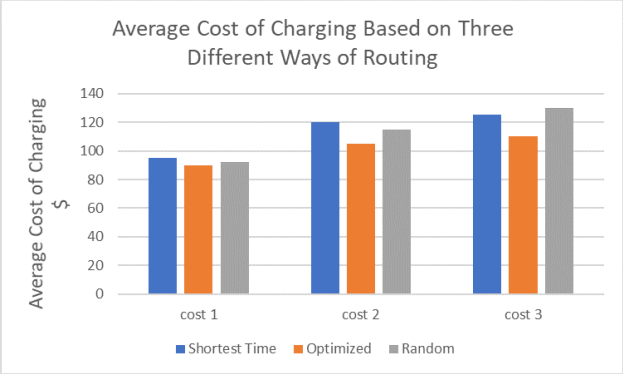

Figure 3.12: Comparison of the charging costs of the three tested schemes.

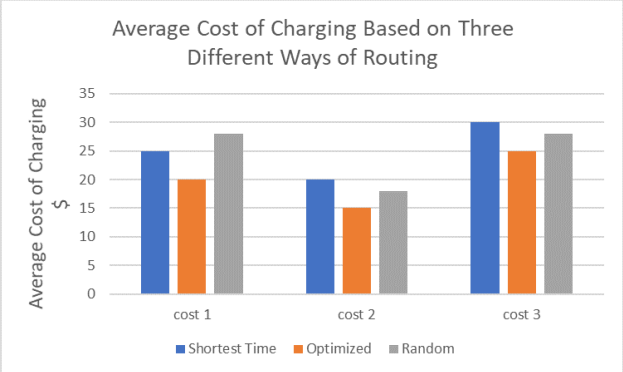

Figure 3.13: Comparison of the total charging costs of the three tested schemes.

3.4.3 Real-World Scenario

In this section, we present the results of implementing our proposed routing optimization approach with M/M/r_k CS model for the real-world PSs of Autolib, the well-known current MoD provider in Paris [33] as in Section 2.4.3, all shown in Figure 2.11. The departure rates from PSs 1-10 are set to 11, 13, 12, 11, 12, 12, 12, 12, 12, 16 EVs/hour. The charging rates at all CSs are set to 21 EVs/hour (i.e. $\mu_k^r = 10$ EVs/hour and $\mu_k^g = 11$ EVs/hour $\forall k$) with 2 charging units at each CS (i.e. $r_k = 2\ \forall k$). The charging costs from the grid are set as follow $r_1 = r_2 = 1$ cost unit/EV and $r_3 = 1.5$ cost unit/EV. Our proposed method is tested and compared to other routing schemes as shown in Figure 3.13. The model is still outperforming the shortest path and random schemes even in a real-world scenario.

3.4.4 Computation Times

As in Section 2.4.4, Computation times are calculated for this proposed model also due to the high execution times known for solving optimization problems. The total number of variables to be calculated in our model is $2 \times n \times (n-1) \times$ m. The calculations are done on the same environment as in Section 2.4.4. Table 3.2 shows the average execution times and the number of variables for the three different cases discussed in the simulation results. As we can see, even though the M/M/1 model and M/M/r_k one have the same number of variables and equations, we see that M/M/r_k model has higher execution time due to the complexity of the equations in the problem. The real-world example has a higher execution time due to the number of variables and equations. As the number of PSs and CSs increase, the execution time will increase as well. Since the optimal routing proportions are assumed to be calculated in time span of one hour or 30 minutes, the execution time will be within the time span.

Table 3.2: Computation times and number of variablesfor all case studies.

	M/M/1 CS Model	**M/M/r_k CS Model**	**Real-World Scenario**
Total Number of Variables	72	72	540
Execution Time (seconds)	3.1	3.34	11.82

CHAPTER 4

Optimal Local and In-Route Charging Management of MoD-EV Systems

In this chapter, we discuss a model similar to the one in chapter 2. However, it is assumed here that there are charging facilities at both the pick-up locations and some other locations around the city. Obviously, charging all EVs at the pick-up locations might not be the best solution as the delay on that charging station may go large or even unbounded and thus some customers should be routed to other charging stations with an objective of minimizing the average total trip time for all the customers. In both chapters 2 and 3, we did not consider the traffic congestion as part of the optimization problem which will be considered in this chapter. For simplicity, we will implement this new setting on the M/M/c queues only as we have seen very similar results for both types of queues in the previous chapters.

4.1 System Model

Similar to Sections 2.1 and 3.1, this section considers a MoD-EV system as shown in Figure 2.1, with n passenger stations (PSs), m charging stations (CSs) around the city (i.e. their locations are different from the locations of PSs) and n charging stations at the PSs (i.e. each PS has a charging station) and are abbreviated as CSP. Customers pick-up/ drop-off EVs close to their origins and destinations, respectively and these locations called PSs. The model only considers EVs that need charging before reaching to the destination by less time-constrained customers, as illustrated by the PS queues in Figure 2.1. Similar to Sections 2.1 and 3.1, the overall departure rate of these EVs from PS i is modeled by a Poisson process with rate λ_i EVs / unit time. When departing, each customer intends to go to PS j with probability q_{ij} ($q_{ii} = 0$). On the other hand, each server at CS k can complete either the direct EV charging or the swapping of its battery [11], [18] in an exponentially distributed duration with rate μ_k EVs / unit and each server at CSP i complete the charging with rate ρ_i

EVs / unit time at PS i, which are different from one charging station to another given their different supplies of energy. The total number of charging units at each CS or CSP is denoted by c. In addition, the real-time trip duration between PSs i and j through CS k, without charging, is denoted by $t_{ij}^{(k)}$ while t_{ij} represents the time spent on the road only between PS i and PS j when EVs charge at CSP i (i.e. it is the shortest path). Another important factor in the model is traffic capacity on each road which is represented by current traffic capacity ($CTC_{ij}^{(k)}$) and maximum traffic capacity ($MTC_{ij}^{(k)}$), respectively. CTC represents the current number of cars in each route while MTC represents the maximum number that will not increase the trip time without charging (i.e. sending more cars will not increase the congestion or the delay on the route). Table 4.1 shows all the parameters considered in our model.

Having a cloud controller that is capable of collecting all the system parameters in real-time given time-varying charging and traffic conditions (and thus time-varying of μ_k, ρ_i, t_{ij}, $t_{ij}^{(k)}$, CTC_{ij}, $CTC_{ij}^{(k)}$, MTC_{ij} and $MTC_{ij}^{(k)}$ $\forall\ i, j, k$), this controller is required to guide each EV departing from PS i towards PS j to charge either at the PS i (origin) or charge in the route at CS k with probabilities P_{ij} and $P_{ij}^{(k)}$, respectively. It is easy to see that:

$$\left(\sum_{k=1}^{m} P_{ij}^{(k)}\right) + P_{ij} = q_{ij}\ \forall\ i, j \text{ and } i \neq j \tag{4.1}$$

$$\sum_{\substack{j=1 \\ i \neq j}}^{n} \sum_{k=1}^{m} \left(P_{ij}^{(k)} + P_{ij}\right) = 1\ \forall\ i \tag{4.2}$$

The EVs departing from all PSs are required to charge at CS k or CSP i and thus they queue up at the stations, thus having additional delays in these CSs and CSPs on top of the actual trip times $t_{ij}^{(k)}$ and t_{ij} without charging. After departing from the CSP or CS, EVs continue their ways to the destination PSs.

This controller is thus required to determine these proportions P_{ij} and P_{ij} periodically, given the real-time values of λ_i, q_{ij}, μ_k, ρ_i, t_{ij}, $t_{ij}^{(k)}$, CTC_{ij}, $CTC_{ij}^{(k)}$, MTC_{ij} and $MTC_{ij}^{(k)}$

Table 4.1: List of System and Decision Parameters

Parameter	**Definition**
n:	Total number of PSs and total number of CSPs
m:	Total number of CSs
λ_i:	Departure rate from PS i
q_{ij}:	Probability for customer to go from PS i to PS j
μ_k, ρ_i:	Charging or battery-swapping rate of each server (charging unit) at CS k and CSP i, respectively
c:	The number of servers (or charging units) at each CS or CSp
$t_{ij}^{(k)}$:	Time spent on the road only from PS i to PS j through CS k without considering the charging time
$P_{ij}^{(k)}$:	Decision routing probability to go from PS i to PS j through CS k
t_{ij}:	Time spent on the road only from PS i to PS j when EV is charged at PS i without considering the charging time (shortest path)
P_{ij}:	Decision routing probability to go from PS i to PS j when EV is charged at PS i
$CTC_{ij}^{(k)}$:	Current number of cars on the route from PS i to PS j through CS k and labeled CTC_{ij} when EV is charged at the origin
$MTC_{ij}^{(k)}$:	Maximum number of cars on the route from PS i to PS j through CS k that will not increase the delay on driving and labeled CTC_{ij} when EV is charged at the origin
$T_{ij}, T_{ij}^{(k)}$:	Upper bounds on the total trip time including charging delays

$\forall\, i, j, k$, in order to optimize the average total trip time for all customers through any route relative to its shortest path (i.e. t_{ij} value $\forall\, i, j, k$). Obviously, the conventional shortest path routing strategy, which routes a customer departing from pick-up location i and destined to drop-off location j through charging at the PS i (i.e. charging at CSP i) may not be the best routing scheme since the CSP may have a huge load (i.e. overloaded) or have low energy resources, and thus results in a large (or even unbounded charging delay) at the charging station. So, the cloud controller should periodically be able to calculate the routing proportions that minimize the overall average trip time for all the customers in each period.

4.2 Problem Formulation

4.2.1 Queuing System Stability Conditions

Using the system model described above, and the thinning property of Poisson processes, the arrival process to the queue of each CS k can be represented by an independent Poisson process with rate λ_k, which is shown by equation (4.3). Similarly, equation (4.4) shows the arrival rate at each CSP i.

$$\lambda_k = \sum_{\substack{i=1 \\ i \neq j}}^{n} \sum_{j=1}^{n} \lambda_i P_{ij}^{(k)} \tag{4.3}$$

$$\lambda_{i_{CSP}} = \sum_{\substack{i=1 \\ i \neq j}}^{n} \sum_{j=1}^{n} \lambda_i P_{ij} \tag{4.4}$$

These expressions are obtained for each charging station by the summation of all thinned departure processes from each PS i whose rates are $\lambda_i P_{ij}^{(k)}$ and $\lambda_i P_{ij}$ as in equations (4.3) and (4.4), respectively. Since the arrival process to each charging station is Poisson with rates λ_k and $\lambda_{i_{CSP}}$, and the charging time at each server is exponentially distributed with rates μ_k and ρ_i and c servers are available at each station , the overall queuing system becomes an M/M/c queue at each CSP i and CS k [26]. Consequently, the entire system becomes a multi-server queuing system consisting of n independent CSP M/M/c and m CS M/M/c queues, with different arrival rates depending on the decision probabilities $P_{ij}^{(k)}$ and P_{ij}, $\forall\ i, j, k$, and different service (or charging) rates due to energy supplies at each station. To ensure the stability of the whole system, the arrival rate to each CS k or CSP i must be strictly less than its total service (charging) rate $c\mu_k$ or $c\rho_i$. These are represented by:

$$\sum_{\substack{i=1 \\ i \neq j}}^{n} \sum_{j=1}^{n} \lambda_i P_{ij}^{(k)} < c\mu_k \ \forall\ k \tag{4.5}$$

$$\sum_{\substack{i=1 \\ i \neq j}}^{n} \sum_{j=1}^{n} \lambda_i P_{ij} < c\rho_i \ \forall \ i \tag{4.6}$$

4.2.2 Problem Statement

The average charging time (denoted by D_k) at each CS k can be represented by equation (4.7) [28]. Also, the average charging time at each CSP i (denoted by D_i) is expressed by equation (4.8) [28].

$$D_k = \frac{1}{(c\mu_k - \lambda_k)\left(1 + \left(1 - \frac{\lambda_k}{c\mu_k}\right)\left(\frac{c!}{(\lambda_k/\mu_k)^c}\right)\left(\sum_{h=0}^{c-1} \frac{(\lambda_k/\mu_k)^h}{h!}\right)\right)} + \frac{1}{\mu_k} \ \forall \ k \tag{4.7}$$

$$D_i = \frac{1}{(c\rho_i - \lambda_k)\left(1 + \left(1 - \frac{\lambda_{i_{CSP}}}{c\mu_k}\right)\left(\frac{c!}{(\lambda_{i_{CSP}}/\rho_i)^c}\right)\left(\sum_{h=0}^{c-1} \frac{(\lambda_{i_{CSP}}/\mu_k)^h}{h!}\right)\right)} + \frac{1}{\rho_i} \ \forall \ i \tag{4.8}$$

Consequently, the total average trip time (denoted by $\tau_{ij}^{(k)}$) from PS i to PS j through CS k with in-route charging can be expressed as:

$$\tau_{ij}^{(k)} = t_{ij}^{(k)} + D_k \ \forall \ i, j, k \tag{4.9}$$

In addition, the total average trip time from PS i to PS j when EV is charged at CSP i before leaving the origin (denoted by τ_{ij}) can be represented as:

$$\tau_{ij} = t_{ij} + D_i \ \forall \ i, j \tag{4.10}$$

As mentioned earlier, the objective of our decision proportions optimization is to minimize the average overall trip time for all customers over all routes relative to their actual trip time without charging, while maintaining the stability of the system. This problem can be

formulated as in (4.11). Constraints (4.11b) and (4.11c) with the objective function guarantee the achievement of the desired goal (minimizing $\tau_{ij}^{(k)}$ and τ_{ij} relative to t_{ij}) in a weighted epigraph form [27]. Since the reciprocal of the delay functions D_k and D_i are concave functions [29] for constant u_k, ρ_i and c, and since the reciprocal of a positive concave function is convex [30], then Constraints (4.11b) and (4.11c) are convex. Constraints (4.11d) and (4.11e) guarantee the stability at each charging queue while constraints (4.11f) and (4.11g) respect the traffic congestion at each route (i.e. guarantee that no more delay will be added in the travel time). Constraints (4.11h) and (4.11i) represent the facts on the proportions $P_{ij}^{(k)}$, P_{ij} in (4.1) and (4.2), respectively. Constraint (4.11j) guarantees that the decision probability is always between 0 and $q_{ij}^{(k)}$ while Constraint (4.11k) guarantees the positivity of the charging delays D_k and D_i. All the constraints in the optimization problem (4.11) are linear except (4.11b) and (4.11c) which are convex. In addition, the objective function is linear. Consequently, the problem in (4.11) becomes a convex optimization problem with

linear cost function and a set of convex constraints.

$$\underset{P_{ij}^{(k)},P_{ij},T_{ij}^{(k)},T_{ij}\ \forall i,j,k}{\text{minimize}} \quad \sum_{\substack{i=1\\i\neq j}}^{n}\sum_{j=1}^{n}\left(\frac{T_{ij}}{t_{ij}}+\sum_{k=1}^{m}\frac{T_{ij}^{(k)}}{t_{ij}}\right) \tag{4.11a}$$

$$s.t. \quad t_{ij}^{(k)}+D_k \leq T_{ij}^{(k)}\ \forall\ i,j,k \tag{4.11b}$$

$$t_{ij}+D_i \leq T_{ij}\ \forall\ i,j \tag{4.11c}$$

$$\sum_{\substack{i=1\\i\neq j}}^{n}\sum_{j=1}^{n}\lambda_i P_{ij}^{(k)} < c\mu_k\ \forall\ k \tag{4.11d}$$

$$\sum_{\substack{i=1\\i\neq j}}^{n}\sum_{j=1}^{n}\lambda_i P_{ij} < c\rho_i\ \forall\ i \tag{4.11e}$$

$$CTC_{ij}^{(k)}+\sum_{\substack{i=1\\i\neq j}}^{n}\sum_{j=1}^{n}\lambda_i P_{ij}^{(k)} \leq MTC_{ij}^{(k)}\ \forall\ i,j,k \tag{4.11f}$$

$$CTC_{ij}+\sum_{\substack{i=1\\i\neq j}}^{n}\sum_{j=1}^{n}\lambda_i P_{ij} \leq MTC_{ij}\ \forall\ i,j \tag{4.11g}$$

$$\left(\sum_{k=1}^{m}P_{ij}^{(k)}\right)+P_{ij}=q_{ij}\ \forall\ i,j \tag{4.11h}$$

$$\sum_{\substack{j=1\\i\neq j}}^{n}\sum_{k=1}^{m}\left(P_{ij}^{(k)}+P_{ij}\right)=1\ \forall\ i \tag{4.11i}$$

$$0 \leq P_{ij}^{(k)}, P_{ij} \leq q_{ij}\ \forall\ i,j,k \tag{4.11j}$$

$$T_{ij}^{(k)}, T_{ij} > t_{ij}^{(k)}, t_{ij}\ \forall\ i,j,k \tag{4.11k}$$

4.3 Analytical Derivation of Optimal Routing

The problem in (4.11) is a convex optimization problem and it satisfies also Slater's theorem. Hence, strong duality holds and the optimal solutions of the primal (original) and dual problems are identical [27]. The Karush-Kuhn-Tucker (KKT) conditions provide necessary and sufficient conditions for optimality [27]. The Lagrangian function of the problem

in (4.11) is given by equation (4.12), where $\alpha_{ij}^{(k)}$, β_{ij}, η_k γ_i, $\omega_{ij}^{(k)}$, ζ_{ij}, χ_{ij}, ψ_i, $\nu_{ij}^{(k)}$, ν_{ij}, $\xi_{ij}^{(k)}$, ξ_{ij}, $\sigma_{ij}^{(k)}$ and σ_{ij} are the Lagrange multipliers of the different problem constraints. The equations (4.13) are derived by applying the KKT conditions on the equality and inequality constraints (4.11b)-(4.11k).

$$
\begin{aligned}
L(P,T,\alpha,\beta,\eta,\gamma,\omega,\zeta,\chi,\psi,\nu,\xi,\sigma) &= \sum_{\substack{i=1\\ i\neq j}}^{n}\sum_{j=1}^{n}\left(\frac{T_{ij}}{t_{ij}}+\sum_{k=1}^{m}\frac{T_{ij}^{(k)}}{t_{ij}}\right)+\sum_{\substack{i=1\\ i\neq j}}^{n}\sum_{j=1}^{n}\sum_{k=1}^{m}\left(\alpha_{ij}^{(k)}\left(t_{ij}^{(k)}+D_k-T_{ij}^{(k)}\right)\right)\\
&+\sum_{\substack{i=1\\ i\neq j}}^{n}\sum_{j=1}^{n}\sum_{k=1}^{m}\left(\beta_{ij}\left(t_{ij}+D_i-T_{ij}\right)\right)+\sum_{k=1}^{m}\eta_k\left(\sum_{\substack{i=1\\ i\neq j}}^{n}\sum_{j=1}^{n}\lambda_i P_{ij}^{(k)}-c\mu_k\right)+\sum_{i=1}^{n}\gamma_i\left(\sum_{\substack{i=1\\ i\neq j}}^{n}\sum_{j=1}^{n}\lambda_i P_{ij}-c\rho_i\right)\\
&+\sum_{\substack{i=1\\ i\neq j}}^{n}\sum_{j=1}^{n}\sum_{k=1}^{m}\left(\omega_{ij}^{(k)}\left(CTC_{ij}^{(k)}+\sum_{\substack{i=1\\ i\neq j}}^{n}\sum_{j=1}^{n}\lambda_i P_{ij}^{(k)}-MTC_{ij}^{(k)}\right)\right)+\sum_{\substack{i=1\\ i\neq j}}^{n}\sum_{j=1}^{n}\left(\chi_{ij}\left(\left(\sum_{k=1}^{m}P_{ij}^{(k)}\right)+P_{ij}-q_{ij}\right)\right)\\
&+\sum_{\substack{i=1\\ i\neq j}}^{n}\sum_{j=1}^{n}\left(\zeta_{ij}\left(CTC_{ij}+\sum_{\substack{i=1\\ i\neq j}}^{n}\sum_{j=1}^{n}\lambda_i P_{ij}^{(k)}-MTC_{ij}\right)\right)+\sum_{i=1}^{n}\left(\psi_i\left(\sum_{\substack{j=1\\ i\neq j}}^{n}\sum_{k=1}^{m}\left(P_{ij}^{(k)}+P_{ij}\right)-1\right)\right)\\
&+\sum_{\substack{i=1\\ i\neq j}}^{n}\sum_{j=1}^{n}\sum_{k=1}^{m}\left(\nu_{ij}^{(k)}\left(P_{ij}^{(k)}-q_{ij}\right)\right)+\sum_{\substack{i=1\\ i\neq j}}^{n}\sum_{j=1}^{n}\left(\nu_{ij}\left(P_{ij}-q_{ij}\right)\right)+\sum_{\substack{i=1\\ i\neq j}}^{n}\sum_{j=1}^{n}\sum_{k=1}^{m}\left(-\xi_{ij}^{(k)}P_{ij}^{(k)}\right)+\sum_{\substack{i=1\\ i\neq j}}^{n}\sum_{j=1}^{n}\left(-\xi_{ij}P_{ij}\right)\\
&+\sum_{\substack{i=1\\ i\neq j}}^{n}\sum_{j=1}^{n}\sum_{k=1}^{m}-\sigma_{ij}^{(k)}\left(T_{ij}^{(k)}-t_{ij}^{(k)}\right)+\sum_{\substack{i=1\\ i\neq j}}^{n}\sum_{j=1}^{n}-\sigma_{ij}\left(T_{ij}-t_{ij}\right)
\end{aligned}
\tag{4.12}
$$

$$\alpha_{ij}^{(k)^*}\left(t_{ij}^{(k)}+D_k-T_{ij}^{(k)^*}\right)=0\ \forall\ i,j,k \tag{4.13a}$$

$$\beta_{ij}^{*}\left(t_{ij}+D_i-T_{ij}^{*}\right)=0\ \forall\ i,j \tag{4.13b}$$

$$\eta_k^*\left(\sum_{\substack{i=1\\ i\neq j}}^{n}\sum_{j=1}^{n}\lambda_i P_{ij}^{(k)^*}-c\mu_k\right)=0\ \forall\ k \tag{4.13c}$$

$$\gamma_i^*\left(\sum_{\substack{i=1\\ i\neq j}}^{n}\sum_{j=1}^{n}\lambda_i P_{ij}^{*}-c\rho_i\right)=0\ \forall\ i \tag{4.13d}$$

$$\omega_{ij}^{(k)^*}\left(CTC_{ij}^{(k)}+\sum_{\substack{i=1\\ i\neq j}}^{n}\sum_{j=1}^{n}\lambda_i P_{ij}^{(k)^*}-MTC_{ij}^{(k)}\right)=0\ \forall\ i,j,k \tag{4.13e}$$

$$\zeta_{ij}^{*}\left(CTC_{ij}^{(k)}+\sum_{\substack{i=1\\ i\neq j}}^{n}\sum_{j=1}^{n}\lambda_i P_{ij}^{*}-MTC_{ij}^{(k)}\right)=0\ \forall\ i,j,k \tag{4.13f}$$

$$\left(\sum_{k=1}^{m}P_{ij}^{(k)^*}\right)+P_{ij}^{*}-q_{ij}=0\ \forall\ i,j \tag{4.13g}$$

$$\sum_{\substack{j=1\\ i\neq j}}^{n}\sum_{k=1}^{m}\left(P_{ij}^{(k)^*}+P_{ij}^{*}\right)-1=0\ \forall\ i \tag{4.13h}$$

$$\nu_{ij}^{(k)^*}\left(P_{ij}^{(k)^*}-q_{ij}\right)=0,\ \nu_{ij}^{*}\left(P_{ij}^{*}-q_{ij}\right)=0,\ \forall\ i,j,k \tag{4.13i}$$

$$-\xi_{ij}^{(k)^*}P_{ij}^{(k)^*}=0,\ \ -\xi_{ij}^{*}P_{ij}^{*}=0,\ \forall\ i,j,k \tag{4.13j}$$

$$-\sigma_{ij}^{(k)^*}\left(T_{ij}^{(k)^*}-t_{ij}^{(k)}\right)=0,\ \sigma_{ij}^{*}\left(T_{ij}^{*}-t_{ij}\right)=0,\ \forall\ i,j,k \tag{4.13k}$$

$$\alpha_{ij}^{(k)^*},\beta_{ij}^{(k)^*},\eta_k^*,\gamma_i^*,\omega_{ij}^{(k)^*},\zeta_{ij}^*,\nu_{ij}^{(k)^*},\xi_{ij}^{(k)^*},\sigma_{ij}^{(k)^*}\geq 0 \tag{4.13l}$$

We can easily see that η_k^*, γ_i^*, $\sigma_{ij}^{(k)^*}$ and σ_{ij}^* are all equal to zero since the second term in equations (4.13c), (4.13d) and (4.13k) is never equal to zero. From (2.10), and since the gradient of the Lagrangian function equals 0 at the optimal solution, we obtain the following

set of equations (4.14a) and (4.14b) for $T_{ij}^{(k)^*}$ and T_{ij}^*, respectively:

$$\frac{1}{t_{ij}} - \alpha_{ij}^{(k)^*} = 0 \ \forall \ i, j, k \tag{4.14a}$$

$$\frac{1}{t_{ij}} - \beta_{ij}^* = 0 \ \forall \ i, j \tag{4.14b}$$

The above equations lead to the optimal values of $\alpha_{ij}^{(k)^*}$ and β_{ij}^*, which are expressed as:

$$\alpha_{ij}^{(k)^*} = \beta_{ij}^* = \frac{1}{t_{ij}} > 0 \ \forall \ i, j, k \tag{4.15}$$

From expressions (4.13a), (4.13b) and the fact that $\alpha_{ij}^{(k)^*}, \beta_{ij}^* > 0$, we can easily find the optimal solution of $T_{ij}^{(k)^*}$ and T_{ij}^*, which are represented by equations (4.16) and (4.17). These two equations show that both $T_{ij}^{(k)^*}$ and T_{ij}^* are exact bounds on the actual trip time.

$$T_{ij}^{(k)^*} = t_{ij}^{(k)} + D_k \ \forall \ i, j, k \tag{4.16}$$

$$T_{ij}^* = t_{ij} + D_i \ \forall \ i, j \tag{4.17}$$

The optimal value of $P_{ij}^{(k)^*}$ can be obtained using the approach of $T_{ij}^{(k)^*}$ and T_{ij}^*. By using equation (4.12) and its gradient, we obtain equation (4.18). The optimal routing decisions $P_{ij}^{(k)^*}$ could be found be solving equation (4.18) for $P_{ij}^{(k)}$. Also, the optimal solution for P_{ij}^* could also be found by solving equation (4.18) for P_{ij}^* but with replacing $P_{ij}^{(k)^*}$ and μ_k by P_{ij}^* and ρ_i, respectively.

Finally, the optimal solutions for the Lagrangian function are the same as the optimal values of the original problem due to the strong duality we have [27].

4.4 Simulation Results

Similar to Sections 2.4 and 3.4, 4 PSs and 3 CSs simulation model is considered. Table 2.2 shows the values of $t_{ij}^{(k)}$ (time on the road only without charging) used in the simulations for

$$\chi_{ij}^{*} + \psi_{i}^{*} + \nu_{ij}^{(k)^{*}} - \xi_{ij}^{(k)^{*}} + \left(\sum_{\substack{i=1 \\ i \neq j}}^{n} \sum_{j=1}^{n} \omega_{ij}^{(k)^{*}} \right) \lambda_i + \left(\sum_{\substack{i=1 \\ i \neq j}}^{n} \sum_{j=1}^{n} \alpha_{ij}^{(k)^{*}} \right) \times$$

$$\left(\frac{\lambda_i q - (c\mu_k - \lambda_k) \left(\frac{-\lambda_i}{c\mu_k} \left(\frac{c!}{a^c} \right) \sum_{h=0}^{c-1} \left(\frac{a^h}{h!} \right) - \frac{c\lambda_i}{\mu_k} \frac{c!}{a^{c+1}} \left(1 - \frac{a}{c} \right) \sum_{h=0}^{c-1} \left(\frac{a^h}{h!} \right) + \frac{\lambda_i}{\mu_k} \left(1 - \frac{a}{c} \right) \left(\frac{c!}{a^c} \right) \sum_{h=1}^{c-1} \left(\frac{a^h}{h!} \right) \right)}{q^2} \right) = 0$$

$$where\ \lambda_k = \sum_{\substack{i=1 \\ i \neq j}}^{n} \sum_{j=1}^{n} \lambda_i P_{ij}^{(k)^{*}}\ ,\ a = \frac{\lambda_k}{\mu_k}\ and\ q = \left(c\mu_k - \lambda_k \right) \left(1 + \left(1 - \frac{a}{c} \right) \left(\frac{c!}{a^c} \right) \sum_{h=0}^{c-1} \frac{a^h}{h!} \right) \quad (4.18)$$

all possible combinations of origins and destinations. Uniform destination PS probabilities are assumed from each origin PS (i.e. $q_{ij} = 1/3\ \forall\ i \neq j$). The type of charging used in the following simulations is the conventional one. Given this model, the optimal routing proportions $P_{ij}^{(k)},\ P_{ij},\ \forall\ i, j, k$ are first illustrated for a wide range of system parameters. The expected total trip time performance achievable by our proposed model is also tested through simulations, and compared to the conventional shortest path scheme (i.e. letting all the EVs charge at the PS and then take the shortest route to the destination), and random routing strategy, i.e., the scheme assigning random values to $P_{ij}^{(k)}$, P_{ij} (non-optimize scheme). Due to space limitation, we will only discuss the results for PS 1 as an example. In all the following simulations, the values of CTC and MTC are set to 3 and 15 EVs for all the available routes.

Figure 4.1 shows the behavior of the routing proportion variables P_{12} and $P_{12}^{(1)}$ as a function of the charging rates $\mu_1,\ \mu_2,\ \mu_3$ and ρ_1 while keeping the departure rate from each of the PSs 1-4 set to 100, 100, 50 and 50 EVs/hour, respectively. For ease of illustration, Table 2.2 shows the without-charging trip time from PS 1 to PS 2 through CS 1 , which is 0.5 hour (i.e. $t_{12}^{(1)}$) and the trip time without charging if the EVs will charge at PS 1 is 0.45 hour (i.e. $t_{12} = 0.45$). We are varying the charging rates at the CSs on one axis (i.e. $\mu_1,\ \mu_2,\ \mu_3$) and the charging rate at PS 1 on the other axis (i.e. ρ_1). As shown in the Figure, the decision $P_{12}^{(1)}$ is higher than P_{12} when the charging rates $\mu_1 = \mu_2 = \mu_3$ are high comparable to μ_1 even though ($t_{12} < t_{12}^{(1)}$). Also, we can see that the decision probability

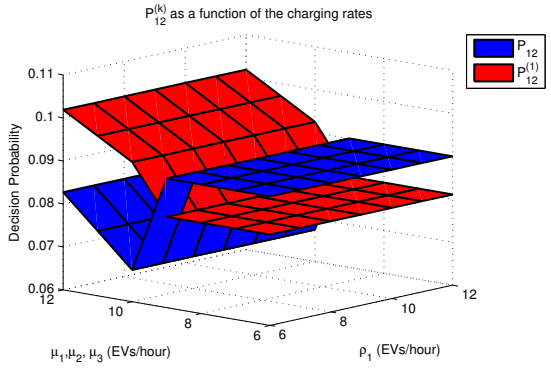

Figure 4.1: Effect of Charging Rate Variation.

P_{12} is higher than $P_{12}^{(1)}$ in the lower mid-range of the left axis (i.e. $6 \leq \mu_1, \mu_2, \mu_3 \leq 9$) even though the value of ρ_1 is small. This happens due to optimality of balancing the loads on the charging stations and avoiding congested routes, which will result in a smaller expected total trip time. None of the decisions reached zero in the Figure, that is due to the optimal balanced on the CSs and CSPs by our proposed method.

Figure 4.2 shows how the routing proportions P_{12} and $P_{12}^{(1)}$ behave when varying the departure rate from PS 1 (λ_1), for fixed departure rates from other PSs. The departure rates from PSs 2-4 are set 100, 50, 50 EVs/hour, respectively and the charging rate at all CSs and CSPs is set to 10 EVs/hour (i.e. $\mu_k = \rho_i = 10\ \forall i, k$). As seen in the Figure, the decision probability P_{12} is much higher than $P_{12}^{(1)}$ when the departure rate is low, that is due to the fact that ($t_{12} < t_{12}^{(1)}$). As the departure rate λ_1 is increasing, P_{12} is decreasing and $P_{12}^{(1)}$ is increasing to balance the load on the charging stations and minimize the average tip time for all the customers. Even with high value of λ_1, P_{12} is still higher than $P_{12}^{(1)}$ because of the travel time on the road without charging. All these variations clearly demonstrate the merits of our cloud-enabled optimization approach due to the high sensitivity of the system behavior (delay) to the real-time values of all the above parameters. Finally, Figure 4.3 compares the trip and charging temporal behaviors of our optimized model with the shortest time path selection and the random routing scheme. In the shortest time strategy, all EVs are charged at their pick-up location and then the customers take the shortest path to the

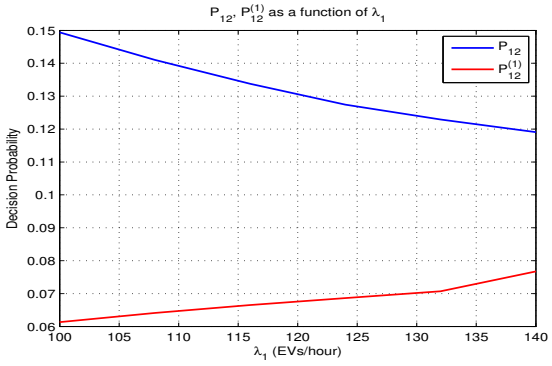

Figure 4.2: Effect of departure rate variations distributions.

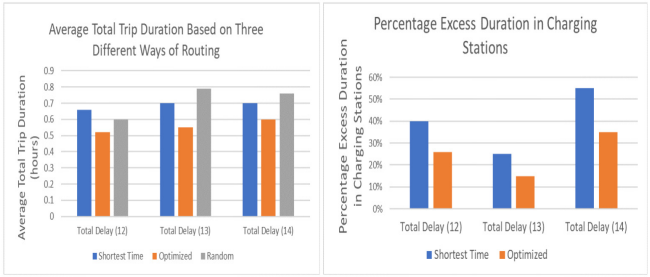

Figure 4.3: Comparison of the trip and charging temporal behaviors of the three tested schemes.

destination while random decisions are assigned to the EVs in case of the random scheme. The departure rates from PSs 1-4 are set to 45, 45, 45, and 45 EVs/hour, respectively, and the charging rates of all CSs and CSPs are set to 10 EVs/hour. The left sub-figure shows the comparison between the three schemes in terms of the average total trip time . As shown, the average total trip time in (Shortest) and (Random) is higher than that of our proposed optimized model for all destinations PSs 2,3, and 4. The right sub-figure shows the percentage excess duration in the charging stations $\left(\text{defined as } (\tau_{ij}^{(k)} - t_{ij}^{(k)})/t_{ij}^{(k)} \times 100\right)$ by our proposed model as compared to the shortest path scheme. As seen, a tremendous gain has been obtained by the use of cloud-enabled routing strategy in comparison to the other schemes of routing.

CHAPTER 5

Summary and Conclusions

In this thesis, we propose a cloud-enabled real-time routing scheme for MoD EVs requiring charging before reaching their destinations. We propose three different models to minimize the average trip times for all the customers relative to their trip times without charging. In the first model, we assume that there is no charging facilities at the pick-up locations and the customers can only perform in-route charging. Hence, it is required to have the minimal increase in their trip times to insure sustainability of such services. We first model the system as a multi-server queuing system using two different models at the CSs, namely M/M/1 and M/M/c queues. Constrained by this models' stability conditions, we formulate the aforementioned problem as two constrained convex problems for the two considered CS models over stochastic routing proportion variables. The analytical expressions for these variables are derived in closed form for the M/M/1 model as well as a solution to a system of equations for the M/M/c model. Furthermore, we plot these optimal routing proportions for a wide variety of system parameters. We also show the significant gains in the trip times and excess charging delays achieved by our optimized routing scheme, compared to the shortest time and random routing schemes, and thus demonstrate its importance in achieving better customer satisfaction. Finally, we test the proposed routing scheme on a real-world scenario and we compute the average execution times for the different discussed settings. In the second model, a cost on the charging is added to the previous model. The objective is to minimize both the travel time as well as the cost of charging. The problem is formulated as a convex optimization problem with two objectives. It is solved then using the same analysis applied on the first model and tested using simulation results to show the performance of the model. In the third model, two options charging are considered either to charge at the pick-up location or perform in-route charging. It is required to know how many customers should charge at the-pick location and how many will perform the in-route one with an objective to minimize the overall expected trip times for all the customers relative to their

trip times without charging. Similar to the previous models, the problem is formulated as a convex optimization problem and is solved again using the Lagrangian analysis and KKT conditions. The model is finally tested through extensive simulations for different system parameters.

For future work, we will extend our study to consider time varying scenarios and then optimize the routing proportions over the current and future arrivals. Moreover, we will consider a more realistic model for the charging stations and take into account its effect on the power grid. Another possible extension is to model the queues at the charging stations using M/M/1/1 and M/M/c/c which prevent the EVs from waiting at the charging stations but may result in high probability of EVs not being served and thus needs a fleet dimensioning and facilities study.

References

[1] M. Ammous, S. Belakaria, S. Sorour, and A. AbdelRahim "Optimal Routing with In-Route Charging of Mobility On-Demand Electric Vehicles, "*in Proc. of IEEE Vehicular Technology Conference (VTC'17-Fall)*, Toronto, ON, Canada, September 2017.

[2] W. J. Mitchell, C. E. Borroni-Bird, and L. D. Burns, "Reinventing the Automobile: Personal Urban Mobility for the 21st Century". Cambridge, MA: The MIT Press, 2010.

[3] D. Schrank, B. Eisele, and T. Lomax, "TTIs 2012 Urban Mobility Report, " *Texas A&M Transportation Institute*, Texas, USA.2012.

[4] U. N. E. Programme, "The Emissions Gap Report 2013 - UNEP, " *Tech. Rep.*, 2013.

[5] "World's Population Increasingly Urban with More than Half Living in Urban Areas, " *United Nations Department of Economic and Social Affairs, Un.org*, 2014. [Online]: http://www.un.org/en/development/desa/news/population/world-urbanization-prospects-2014.html.

[6] R. Zhang and M. Pavone, "Control of Robotic Mobility on-Demand Systems: A Queuing-theoretical Perspective, " *International Journal of Robotics Research archive*, vol. 35, no. 1-3, pp. 186-203, 2016.

[7] H. Jain, K. Kumaraswamy and R. N. Maurya, "Plug-In Electric Vehicles - Distribution System Impacts and High Level Screening Methodologies for Calculating Costs and Benefits, " *ISGT 2014*, 2014,.

[8] T. Zhang, W. Chen, Z. Han and Z. Cao, "Charging Scheduling of Electric Vehicles With Local Renewable Energy Under Uncertain Electric Vehicle Arrival and Grid Power Price, " *IEEE Transactions on Vehicular Technology*, vol. 63, no. 6, pp. 2600-2612, July 2014.

[9] H. Liang, I. Sharma, W. Zhuang and K. Bhattacharya, "Plug-in Electric Vehicle Charging Demand Estimation based on Queuing Network Analysis, " *2014 IEEE PES General Meeting | Conference & Exposition*, 2014.

[10] K. Zhang, Y. Mao, S. Leng, Y. Zhang, S. Gjessing and D. H. K. Tsang,"Platoon-based electric vehicles charging with renewable energy supply: A queuing analytical model, " *2016 IEEE International Conference on Communications (ICC)*, Kuala Lumpur, 2016, pp. 1-6.

[11] X. Tan, B. Sun and D. H. K. Tsang, "Queuing Network Models for Electric Vehicle Charging Station with Battery Swapping, "*IEEE International Conference on Smart Grid Communications (SmartGridComm)*, 2014.

[12] C. H. Ou, H. Liang and W. Zhuang, "Investigating Wireless Charging and Mobility of Electric Vehicles on Electricity Market, " *in IEEE Transactions on Industrial Electronics*, vol. 62, no. 5, pp. 3123-3133, May 2015.

[13] Q. Kang, S. Feng, M. Zhou, A. C. Ammari and K. Sedraoui, "Optimal Load Scheduling of Plug-In Hybrid Electric Vehicles via Weight-Aggregation Multi-Objective Evolutionary Algorithms, " *in IEEE Transactions on Intelligent Transportation Systems,* vol. 18, no. 9, pp. 2557-2568, Sept. 2017.

[14] Q. Kang, J. Wang, M. Zhou and A. C. Ammari, "Centralized Charging Strategy and Scheduling Algorithm for Electric Vehicles Under a Battery Swapping Scenario, " *in IEEE Transactions on Intelligent Transportation Systems,* vol. 17, no. 3, pp. 659-669, March 2016.

[15] J. Barco, A. Guerra, L. Muñoz, and N. Quijano, "Optimal Routing and Scheduling of Charge for Electric Vehicles: Case Study, " 2013. [Online]: https://arxiv.org/abs/1310.0145

[16] C. Kurtulus and G. Inalhan, "Model Based Route Guidance for Hybrid and Electric Vehicles, " *2015 IEEE 18th International Conference on Intelligent Transportation Systems*, Las Palmas, 2015, pp. 1723-1728.

[17] M. Wang, H. Liang, R. Zhang, R. Deng and X. Shen, "Mobility-Aware Coordinated Charging for Electric Vehicles in VANET-Enhanced Smart Grid, " *in IEEE Journal on Selected Areas in Communications,* vol. 32, no. 7, pp. 1344-1360, July 2014.

[18] J.D. Adler, "Routing and Scheduling of Electric and Alternative-Fuel Vehicles, " *PhD Thesis, Arizona State University*, May 2014. [Online]: https://repository.asu.edu/attachments/134788/content/Adler_asu_0010E 13619.pdf

[19] R. Zhang, K. Spieser, E. Frazzoli and M. Pavone, "Models, algorithms, and evaluation for autonomous mobility-on-demand systems, " *2015 American Control Conference (ACC)*, Chicago, IL, 2015, pp. 2573-2587.

[20] M. Drwal, E. Gerding, S. Stein, K. Hayakawa, and H. Kitaoka, "Adaptive pricing mechanisms for on-demand mobility, " in Proceedings of the 16th Conference on Autonomous Agents and MultiAgent Systems, ser. AAMAS '17. Richland, SC: International Foundation for Autonomous Agents and Multiagent Systems, 2017, pp. 1017-1025.

[21] E. S. Rigas, S. D. Ramchurn and N. Bassiliades, "Algorithms for Electric Vehicle Scheduling in Mobility-on-Demand Schemes, " *2015 IEEE 18th International Conference on Intelligent Transportation Systems*, Las Palmas, 2015, pp. 1339-1344.

[22] Cepolina, E. and Farina, A. (2012). A new shared vehicle system for urban areas. *Transportation Research Part C: Emerging Technologies,* 21(1), pp.230-243.

[23] S. Belakaria, M. Ammous, S. Sorour, and A. Abdel-Rahim, "A Multi-Class Dispatching and Charging Scheme for Autonomous Electric Mobility On-Demand, " *in Proc. of IEEE Vehicular Technology Conference (VTC'17-Fall)*, Toronto, ON, Canada, September 2017.

[24] F. Y. Wang, N. N. Zheng, D. Cao, C. M. Martinez, L. Li and T. Liu, "Parallel driving in CPSS: a unified approach for transport automation and vehicle intelligence, " in *IEEE/CAA Journal of Automatica Sinica*, vol. 4, no. 4, pp. 577-587, 2017.

[25] A. Y. S. Lam, K. C. Leung and V. O. K. Li, "Capacity Estimation for Vehicle-to-Grid Frequency Regulation Services With Smart Charging Mechanism, " *in IEEE Transactions on Smart Grid*, vol. 7, no. 1, pp. 156-166, Jan. 2016.

[26] A. Papoulis and S. Pillai, Probability, Random Variables, and Stochastic Processes, 4th ed. International Edition: McGraw-Hill, 2002.

[27] S. Boyd and L. Vandenberghe, Convex optimization, 1st ed. Cambridge: Cambridge University Press, 2015.

[28] A.L. Garcia, Probability, Statistics, and Random Processes for Electrical Engineering, 3rd ed., Prentice Hall, 2008.

[29] A. Harel and P. Zipkin, "Strong Convexity Results for Queueing Systems", *Operations Research*, vol. 35, no. 3, pp. 405-418, 1987.

[30] C. Floudas, *Deterministic global optimization*. New York: Springer, 2011.

[31] C. MACDONALD, "Radical electric car battery can be fully recharged in FIVE minutes", *Daily Mail*, 2017. [Online]. Available: http://www.dailymail.co.uk/sciencetech/article-4508314/Electric-car-battery-fully-charged-FIVE-minutes.html.

[32] Google Maps. (2018). *Google Maps*. [online] Available at: https://www.google.com/maps/

[33] Autolib.eu. (2018). *Autolib'*. [online] Available at: https://www.autolib.eu/stations/

[34] MATLAB and Statistics Toolbox Release 2012a The MathWorks, Inc., Natick, Massachusetts, United States.

[35] Andrews, T. (2012). "Computation Time Comparison Between Matlab and C++ Using Launch Window" [online] Digitalcommons.calpoly.edu. Available at: http://digitalcommons.calpoly.edu/aerosp/78/.

Appendix A: IEEE Copyrights

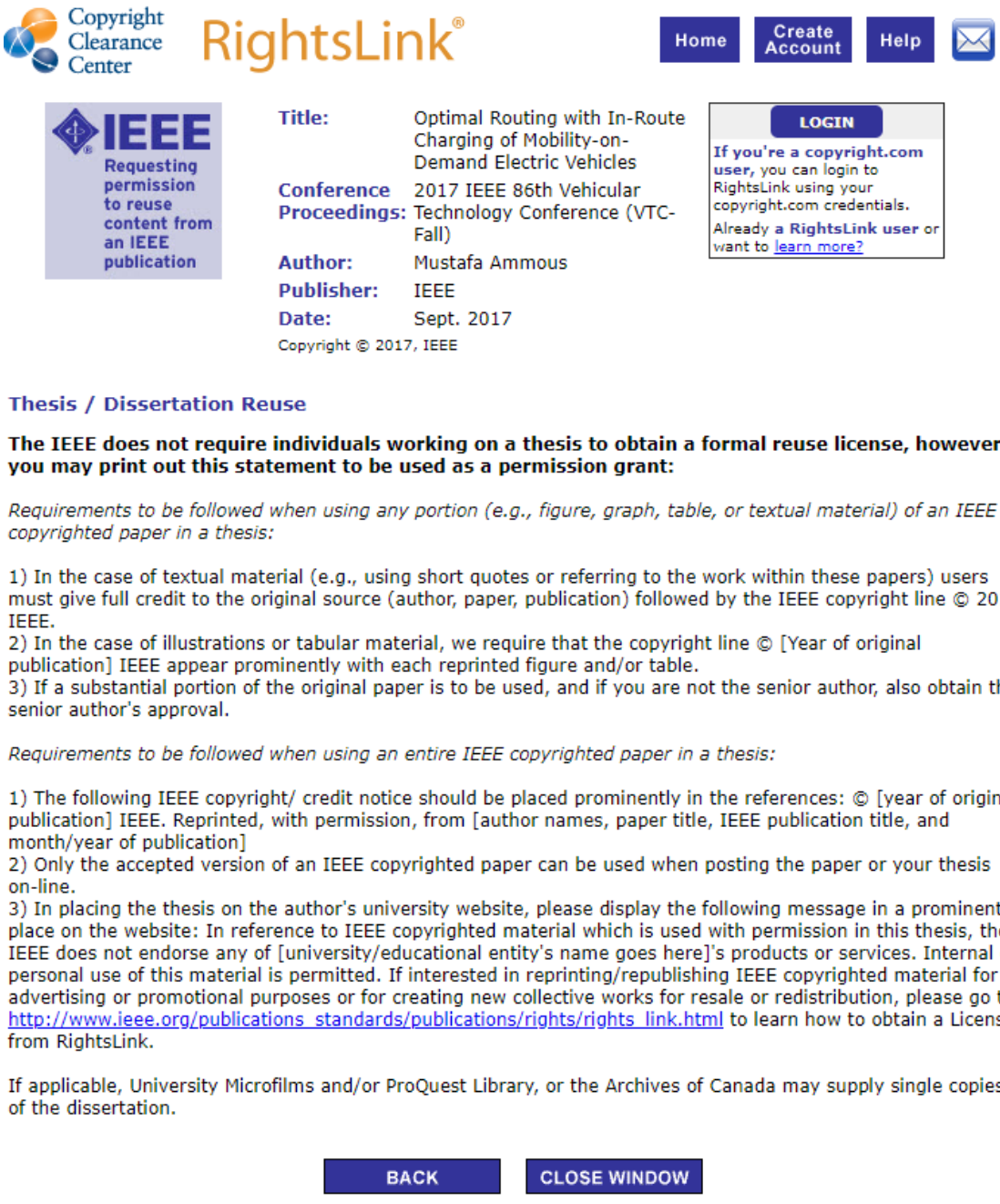

Copyright Clearance Center RightsLink®

Home | Create Account | Help

IEEE Requesting permission to reuse content from an IEEE publication

Title: Optimal Routing with In-Route Charging of Mobility-on-Demand Electric Vehicles
Conference Proceedings: 2017 IEEE 86th Vehicular Technology Conference (VTC-Fall)
Author: Mustafa Ammous
Publisher: IEEE
Date: Sept. 2017
Copyright © 2017, IEEE

LOGIN

If you're a copyright.com user, you can login to RightsLink using your copyright.com credentials.
Already a RightsLink user or want to learn more?

Thesis / Dissertation Reuse

The IEEE does not require individuals working on a thesis to obtain a formal reuse license, however, you may print out this statement to be used as a permission grant:

Requirements to be followed when using any portion (e.g., figure, graph, table, or textual material) of an IEEE copyrighted paper in a thesis:

1) In the case of textual material (e.g., using short quotes or referring to the work within these papers) users must give full credit to the original source (author, paper, publication) followed by the IEEE copyright line © 2011 IEEE.
2) In the case of illustrations or tabular material, we require that the copyright line © [Year of original publication] IEEE appear prominently with each reprinted figure and/or table.
3) If a substantial portion of the original paper is to be used, and if you are not the senior author, also obtain the senior author's approval.

Requirements to be followed when using an entire IEEE copyrighted paper in a thesis:

1) The following IEEE copyright/ credit notice should be placed prominently in the references: © [year of original publication] IEEE. Reprinted, with permission, from [author names, paper title, IEEE publication title, and month/year of publication]
2) Only the accepted version of an IEEE copyrighted paper can be used when posting the paper or your thesis on-line.
3) In placing the thesis on the author's university website, please display the following message in a prominent place on the website: In reference to IEEE copyrighted material which is used with permission in this thesis, the IEEE does not endorse any of [university/educational entity's name goes here]'s products or services. Internal or personal use of this material is permitted. If interested in reprinting/republishing IEEE copyrighted material for advertising or promotional purposes or for creating new collective works for resale or redistribution, please go to http://www.ieee.org/publications_standards/publications/rights/rights_link.html to learn how to obtain a License from RightsLink.

If applicable, University Microfilms and/or ProQuest Library, or the Archives of Canada may supply single copies of the dissertation.

BACK | CLOSE WINDOW